General Disclaimer

One or more of the Following Statements may affect this Document

- This document has been reproduced from the best copy furnished by the organizational source. It is being released in the interest of making available as much information as possible.

- This document may contain data, which exceeds the sheet parameters. It was furnished in this condition by the organizational source and is the best copy available.

- This document may contain tone-on-tone or color graphs, charts and/or pictures, which have been reproduced in black and white.

- This document is paginated as submitted by the original source.

- Portions of this document are not fully legible due to the historical nature of some of the material. However, it is the best reproduction available from the original submission.

COLLEGE OF ENGINEERING

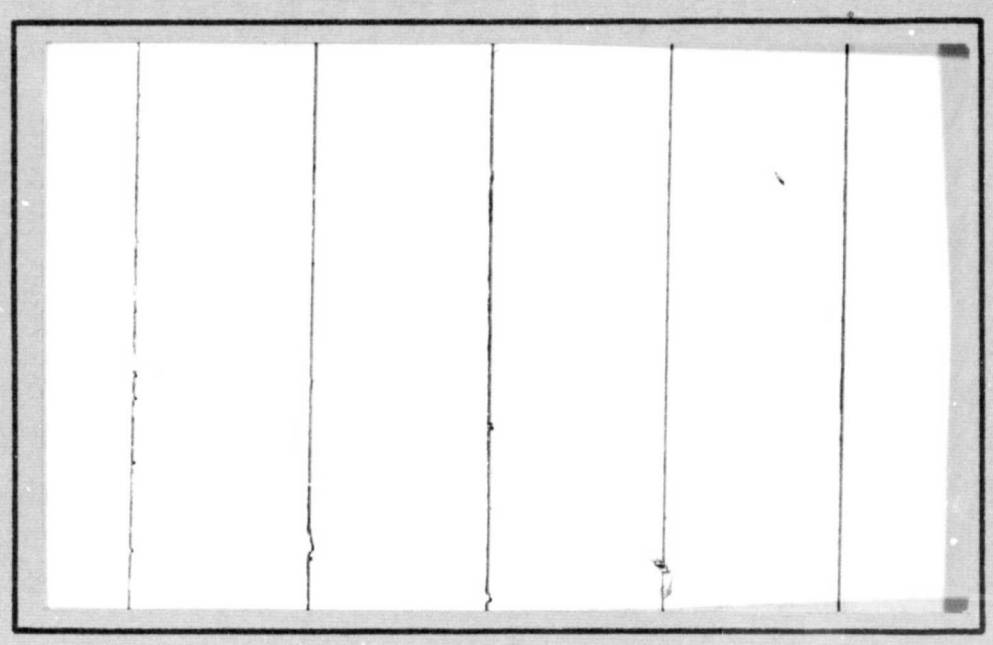

VIRGINIA POLYTECHNIC INSTITUTE AND STATE UNIVERSITY

BLACKSBURG, VIRGINIA

October 1977

THEORY OF ULTRASONIC DIFFRACTION BY DAMAGE DEVELOPED IN THIN LAMINATED COMPOSITES

D. T. HAYFORD
E. G. HENNEKE

ENGINEERING SCIENCE AND
MECHANICS DEPARTMENT

SEMI-ANNUAL STATUS REPORT
NASA GRANT NSG-1254
1 April, 1977 - 30 September 1977

PREPARED FOR:

MATERIALS APPLICATION BRANCH
MANUFACTURING TECHNOLOGY SECTION
NASA LANGLEY RESEARCH CENTER
HAMPTON, VA. 23665

ACKNOWLEDGMENTS

This work is sponsored by the National Aeronautics and Space Administration, Langley Research Center under grant NSG-1254. The authors express their appreciation to Mr. Edward L. Hoffman of NASA Langley and Drs. W. W. Stinchcomb and K. L. Reifsnider of VPI & SU.

ABSTRACT

This report provides a general theory of the diffraction of ultrasonic waves. The theory is then used to find the apparent attenuation which would result if certain damage states (transverse cracks and delaminations) are introduced into a graphite/epoxy laminate through which the ultrasonic wave passes.

Some experimental data for two different laminates ([0, 90, ±45]s and [0, ±45, 90]s) is presented which shows changes in the apparent attenuation of about 1 dB. These changes generally occur at loads which correspond to the range predicted for the formation of the above mentioned damage. Though no exact correlation between theoretical and experimental results is given, the predicted changes in the attenuation for several simple and common damage states are well within the range of experimental values.

It is hoped that the technique described herein can be further developed and used to detect the formation and growth of damage in composite specimens in regions not readily visible by conventional techniques.

TABLE OF CONTENTS

LIST OF FIGURES

LIST OF TABLES

LIST OF SYMBOLS

A, A_0 : Initial amplitude of an ultrasonic pulse

A_1, A_2 : Maximum amplitude of the first and second major echo

A_1, A_2 : Quantities used in evaluating the diffraction integrals

a_i : Gaussian quadrature constant

A_{ij} : Laminate extensional stiffness matrix

B : Bulk modulus of a material

B_{ij} : Coupled bending-extensional stiffness matrix

D_{ij} : Laminate bending stiffness matrix

E_i, E_{ii} : Lamina or laminate Young's Modulus in the i direction

F : Frequency of the ultrasonic pulse

G : Green's function

G_{12} : In-plane shear modulus of a lamina

H_i : Gaussian quadrature constant

H_1, H_2 : Quantities used in evaluating the diffraction integral

I : The value of any integral

k : The wave number

ℓ : Thickness of the bond

L : Length of the buffer block

$\{M\}$: Applied moment resultant

$\vec{n}$: Outward normal to a surface

N : Order of the Gaussian quadrature formula

$\{N\}$: Applied force resultant

$\{N^T\}$: Effective thermal applied resultant

p : Pressure

$\tilde{p}$: Average pressure on a transducer

$\overline{Q}_{ij}$: Transformed reduced stiffness matrix of a lamina

r : A distance from one point to another

R : Radius of the transducer

R_{ij} : Reflection coefficient

S, S' : Surfaces of integration

S : Failure stress of a lamina in shear

T_{ij} : Reflection coefficient

u : Displacement in the x-direction in a laminate

u^o : Midplane displacement in the x-direction

u_i : Particle displacement in the i-direction

u_m, u_n : Maximum displacement of an ultrasonic wave in the m^{th} and n^{th} echoes

v : Variable in Kirchoff's diffraction integral

v : Displacement in the y-direction in a laminate

v^o : Midplane displacement in the y-direction

v' : Undisturbed wave variable

V : Volume of integration

V_b : Velocity of sound in the bond

V_L : Longitudinal wave speed

V_T : Transverse wave speed

w : Angular frequency

w : Vertical displacement of the midplane

x : Failure stress in the 1-direction in a lamina

y : Failure stress in the 2-direction in a lamina

z_i : Acoustic impedance of a material

$\{\alpha\}$: Coefficient of thermal expansion

α : Attenuation coefficient, with various subscripts

β : wave number in the bonding agent

Δ : Dilatation

ϵ : A small length

$\{\epsilon^0\}$: Midplane strain in a laminate

$\{\epsilon\}$: Total strain

$\{\epsilon^M\}$: Mechanical strain

$\{\epsilon^T\}$: Thermal strain

$\{\kappa\}$: Midplane curvatures in a laminate

λ : Lame material constant

μ : Lame material constant

ν_{12} : In-plane Poisson's ratio for a lamina

ρ : Density; radial coordinate

σ, σ' : Surfaces of integration

σ_z : Interlaminar normal stress

$\{\sigma\}$: Two-dimensional stresses at a point

1. INTRODUCTION

In a real sense, the macroscopic behavior of a material is determined by interactions which occur on a microscopic or sub-microscopic level. This is especially true of the failure of a material wherein small local failures gradually intertwine until they produce an effect which is catastrophic for the material, and, quite possibly, to the structure containing that material.

An understanding of the failure of composite laminates, then, must be preceded by an understanding of these microscopic failures; in general, the major types of microscopic damage are transverse cracks and delaminations. Usually, though, only the outermost edge of a specimen can be observed visually, and the need to "observe" the damage interior to a specimen, both during and after the formation of that damage, calls for new methods and techniques in the field of non-destructive testing and engineering.

Several techniques, both new and old, are under investigation at Virginia Polytechnic Institute and State University. Among these are vibrothermography, acoustic emissions, acoustic emission signature analysis, ultrasonic attenuation measurements, and replications. This report investigates the possibility of one more type of ultrasonic testing, where the formation of damage in a composite specimen serves as a rudimentary diffraction grating which causes a change in the apparent attenuation of the specimen.

The underlying purpose here, then, is to serve as a basis for future investigations. This text merely purports to show that such

attenuation changes could be caused by the formation of damage, not that they are caused by such formation. That proof, and the possible application of the method herein described to measuring microscopic failure in composites, will require considerable additional time and effort.

2. LAMINATE PLATE THEORY

The analysis of laminated composite plates under in-plane loads is well documented, and will be only briefly presented here. Readers are referred to [1] for more details.

The simplified theory assumes that each lamina is under a state of two-dimensional stress, and that all displacements are small (Kirchoff-Love hypotheses). The in-plane displacements are given by

$$u(x,y) = u^0(x,y) - z\frac{\partial w(x,y)}{\partial x}$$
$$v(x,y) = v^0(x,y) - z\frac{\partial w(x,y)}{\partial y} \qquad (1)$$

where u and v are the x and y displacements at a point in the laminate; u^0 and v^0 are the x and y displacements of the midplane of the laminate; z is the vertical distance from the midplane to the point; and w is the vertical displacement of the midplane. The coordinate system is shown in Fig. 1. The x-y-z system is the global coordinate system, and is the same for all layers in the laminate. The 1-2-3 system is known as the material coordinate system, and varies from layer to layer. The angle between the 1-axis and x-axis is often used to refer to a particular lamina; thus, a lamina whose angular orientation is 45^0 is often called a 45^0 layer. Material properties are usually expressed in the local (material) system, and then transformed to the global system when necessary.

Differentiation of Eqn. (1) to find the in-plane strains yields:

$$\epsilon_x = \frac{\partial u^0}{\partial x} - z\frac{\partial^2 w}{\partial x^2}$$

continued

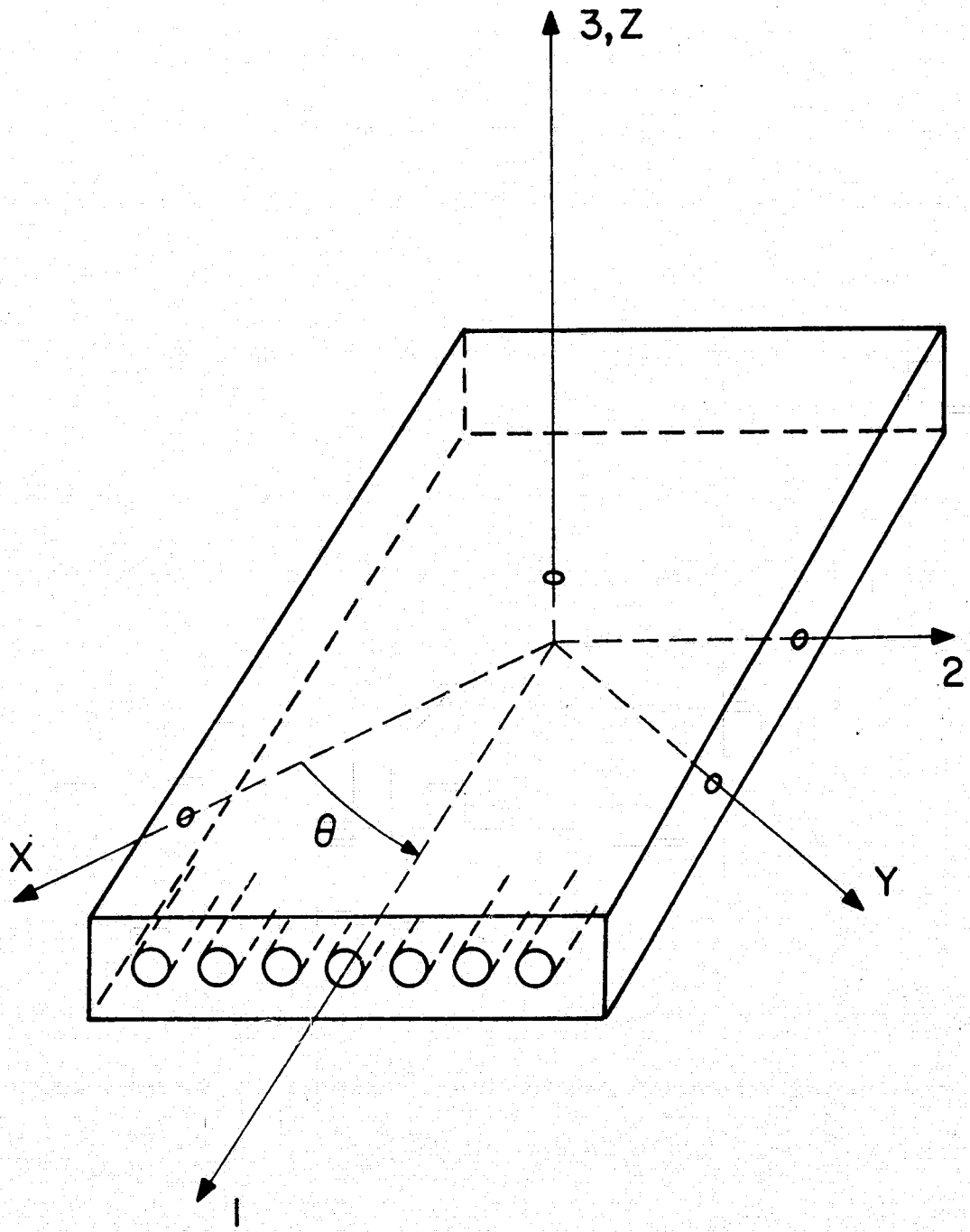

Figure 1
Orientations of Local and Global Coordinate Systems
for a Composite Lamina

$$\varepsilon_y = \frac{\partial v^o}{\partial y} - z\frac{\partial^2 w}{\partial y^2} \tag{2}$$

$$\gamma_{xy} = \frac{\partial u^o}{\partial y} + \frac{\partial v^o}{\partial x} - 2z\frac{\partial^2 w}{\partial x \partial y}$$

The stresses are related to strains by the transformed reduced stiffness matrix, to give

$$\begin{Bmatrix} \sigma_x \\ \sigma_y \\ \tau_{xy} \end{Bmatrix} = \begin{bmatrix} \overline{Q}_{11} & \overline{Q}_{12} & \overline{Q}_{16} \\ \overline{Q}_{12} & \overline{Q}_{22} & \overline{Q}_{26} \\ \overline{Q}_{16} & \overline{Q}_{26} & \overline{Q}_{66} \end{bmatrix} \begin{Bmatrix} \varepsilon_x \\ \varepsilon_y \\ \gamma_{xy} \end{Bmatrix} \tag{3}$$

Thus, the stresses are given by

$$\begin{Bmatrix} \sigma_x \\ \sigma_y \\ \tau_{xy} \end{Bmatrix} = \begin{bmatrix} \overline{Q} \end{bmatrix} \left| \begin{Bmatrix} \varepsilon_x^o \\ \varepsilon_y^o \\ \gamma_{xy}^o \end{Bmatrix} - z \begin{Bmatrix} \kappa_x \\ \kappa_y \\ \kappa_{xy} \end{Bmatrix} \right| \tag{4}$$

where

$$\begin{Bmatrix} \varepsilon_x^o \\ \varepsilon_y^o \\ \gamma_{xy}^o \end{Bmatrix} = \begin{Bmatrix} \partial u^o/\partial x \\ \partial v^o/\partial y \\ \partial u^o/\partial y + \partial v^o/\partial x \end{Bmatrix} \tag{5}$$

are called the midplane strains, and

$$\begin{Bmatrix} \kappa_x \\ \kappa_y \\ \kappa_{xy} \end{Bmatrix} = \begin{Bmatrix} \partial^2 w/\partial x^2 \\ \partial^2 w/\partial y^2 \\ 2\partial^2 w/\partial x \partial y \end{Bmatrix} \tag{6}$$

are called the midplane curvatures.

As in classical plate theory, the stresses and z times the stresses are integrated over the thickness of the plate to obtain the force and moment resultants. Since u^0, v^0, and w are independent of z, these integrations reduce to the integrations of the stiffness matrix across the thickness. The force and moment resultants, in terms of the strains and curvatures are

$$\begin{Bmatrix} N_x \\ N_y \\ N_{xy} \end{Bmatrix} = \begin{bmatrix} A_{11} & A_{12} & A_{16} \\ A_{12} & A_{22} & A_{26} \\ A_{16} & A_{26} & A_{66} \end{bmatrix} \begin{Bmatrix} \varepsilon_x^0 \\ \varepsilon_y^0 \\ \gamma_{xy}^0 \end{Bmatrix} - \begin{bmatrix} B_{11} & B_{12} & B_{16} \\ B_{12} & B_{22} & B_{26} \\ B_{16} & B_{26} & B_{66} \end{bmatrix} \begin{Bmatrix} \kappa_x \\ \kappa_y \\ \kappa_{xy} \end{Bmatrix} \tag{7}$$

$$\begin{Bmatrix} M_x \\ M_y \\ M_{xy} \end{Bmatrix} = \begin{bmatrix} B_{11} & B_{12} & B_{16} \\ B_{12} & B_{22} & B_{26} \\ B_{16} & B_{26} & B_{66} \end{bmatrix} \begin{Bmatrix} \varepsilon_x^0 \\ \varepsilon_y^0 \\ \gamma_{xy}^0 \end{Bmatrix} - \begin{bmatrix} D_{11} & D_{12} & D_{16} \\ D_{12} & D_{22} & D_{26} \\ D_{16} & D_{26} & D_{66} \end{bmatrix} \begin{Bmatrix} \kappa_x \\ \kappa_y \\ \kappa_{xy} \end{Bmatrix} \tag{8}$$

where

$$(A_{ij}, B_{ij}, D_{ij}) = \int_{-\frac{H}{2}}^{\frac{H}{2}} (1, z, z^2)\, \bar{Q}_{ij}\, dz \tag{9}$$

when H is the laminate thickness. If the laminate is symmetric about the midplane, it can be shown that the B matrix is identically zero, reducing Eqns. (7) and (8) to

$$\begin{Bmatrix} N_x \\ N_y \\ N_{xy} \end{Bmatrix} = [A] \begin{Bmatrix} \varepsilon_x^0 \\ \varepsilon_y^0 \\ \gamma_{xy}^0 \end{Bmatrix} \tag{10}$$

and

$$\begin{Bmatrix} M_x \\ M_y \\ M_{xy} \end{Bmatrix} = -[D] \begin{Bmatrix} \kappa_x \\ \kappa_y \\ \kappa_{xy} \end{Bmatrix} \tag{11}$$

Once the midplane strains and curvatures are determined in terms of the applied loads, from either Eqns. (7) and (8), or Eqns. (10) and (11), they are substituted into Eqn. (4) to determine the stresses in each layer. For the case of a symmetric laminate, the stresses in the m^{th} layer when no external moments are applied, are

$$\begin{Bmatrix} \sigma_x \\ \sigma_y \\ \tau_{xy} \end{Bmatrix}_m = [\bar{Q}]_m [A]^{-1} \begin{Bmatrix} N_x \\ N_y \\ N_{xy} \end{Bmatrix} \tag{12}$$

where $[\bar{Q}]_m$ is used to denote the transformed reduced stiffness matrix of the m^{th} layer.

2.1 Curing Stresses

Because the composite laminate is used at temperatures much lower than the temperature at which it was cured, residual internal stresses result from the different expansions and contractions of each layer. These must also be included in the stress analysis of the composite. This becomes especially important when considering damage development in composites, as will be discussed later. Though what follows can be generalized to apply to any laminate, it is developed here only for symmetric laminates.

Since the laminate is symmetric, there will be no bending; hence, the strain in each layer will be the same. This strain is composed of two parts; the free thermal strain, and the strain imposed by the constraints of the other layers. Thus

$$\{\varepsilon^o\} = \{\varepsilon^T\}_k + \{\varepsilon^m\}_k \tag{13}$$

where $\{\varepsilon^o\}$ are the three midplane strains, $\{\varepsilon^T\}_k$, the three thermal strains in the k^{th} layer, and $\{\varepsilon^m\}_k$, the three mechanical strains. Because the mechanical strains arise from the constraints of the other layers, they determine the stresses in each layer, thus

$$\{\sigma\}_k = [\overline{Q}]_k \left[\{\varepsilon^o\} - \{\varepsilon^T\}_k\right] \tag{14}$$

The thermal strains have the form of

$$\begin{Bmatrix} \varepsilon_x^T \\ \varepsilon_y^T \\ \gamma_{xy}^T \end{Bmatrix}_k = \begin{Bmatrix} \alpha_x \\ \alpha_y \\ \alpha_{xy} \end{Bmatrix}_k \Delta T \tag{15}$$

where ΔT is the temperature difference causing the thermal strains, and the α's are the coefficients of thermal expansion of the k^{th} layer.

If there is no net force acting on the laminate, the integral of the stresses across the laminate thickness must be zero. Again, noting that $\{\varepsilon^o\}$ is independent of the z direction, this integral becomes

$$\int_{-\frac{H}{2}}^{\frac{H}{2}} [\bar{Q}]_k \, dz \, \{\varepsilon^0\} - \int_{-\frac{H}{2}}^{\frac{H}{2}} [\bar{Q}]_k \, \{\alpha\}_k \, \Delta T \, dz = 0 \tag{16}$$

Calling the last integral of Eqn. (16) $\{N\}^T$, Eqn. (16) is solved for $\{\varepsilon^0\}$ to give

$$\{\varepsilon^0\} = [A]^{-1} \{N\}^T \tag{17}$$

Equation (14) is then used to solve for the curing stresses in each layer.

2.2 The Pipes-Pagano Interlaminar Normal Stress Approximation

Laminate theory assumes that the entire plate is under a state of two-dimensional stress, and this is essentially true in regions away from the free edges a distance approximately equal to the thickness of the laminate. In these boundary regions, however, significant interlaminar normal stresses (σ_z) exist. Pipes and Pagano [2] have proposed an approximate solution for the normal stress in the boundary region. No details are given here, but the interested reader is invited to refer to their paper. The greatest importance of their approximation is the relative magnitude of the normal stress and its sign (tensile or compressive) through the thickness of the laminate. This will be discussed in more detail later.

3. DAMAGE DEVELOPMENT IN COMPOSITE MATERIALS

The subject of damage development in composites has received much attention, but the phenomenological process remains unexplained for the most part. The discussion presented here is largely conjecture, although supported by some experimental observations.

Two different composite laminates are discussed here. The first, hereafter called type I, has a $[0^{o}, \pm 45^{o}, 90^{o}]_{s}$ stacking sequence. The second, hereafter called type II, has a $[0^{o}, 90^{o}, \pm 45^{o}]_{s}$ stacking sequence. Average lamina properties of the AS-3501 graphite epoxy used in constructing the specimens are presented in Table I.

The two most frequently observed types of damage in composites are transverse cracks and delaminations. Transverse cracks are those which exist parallel to the fiber (1) direction, caused mainly by stresses in the 2 direction (σ_2). Delaminations are separations between laminae caused by interlaminar normal stresses (σ_3). Delaminations are generally confined to a region close to the free edges of a specimen, while transverse cracks are thought to extend across the width of the specimen. Though seemingly unrelated, both types of damage occur because of the relatively low strength of the epoxy used to hold the graphite fibers together.

A computer program was written to calculate the curing stresses for a symmetric laminate, as well as to predict the average laminate properties and the applied resultant (N_x) necessary for the failure of at least one lamina. The failure criterion used was a Tsai-Hill criterion [1] which states that failure occurs when the following condition is

met:

$$\frac{\sigma_1^2}{X^2} - \frac{\sigma_1\sigma_2}{X^2} + \frac{\sigma_2^2}{Y^2} + \frac{\tau_{12}^2}{S^2} = 1 \qquad (18)$$

The values used for X, Y, and S are also presented in Table I. The curing, mechanical, and total stresses at first-ply failure are presented in Table II. Note that the stresses and average laminate properties listed are for both types of laminates, since laminate theory cannot distinguish between their in-plane behavior. Table III presents the results of the Pipes-Pagano approximation of the maximum interlaminar normal stress existing between laminae. Note that these stresses are different for the two laminates. The applied load resultant, N_x, is 875 lbs/in for both tables.

For both laminates, the 90^0 plies fail first, and failure occurs when σ_2 is approximately equal to Y. The curing stress (σ_2^T) for these laminae is 4.77 ksi, and if N_x is 875 lb/in, the total stress (σ_2) in the 90^0 layers is 8.2 ksi, resulting in a predicted total failure of the 90^0 plies by transverse cracking. Experimentally, cracks have been observed to begin at about 900-1000 lbs/in; however, the entire ply does not fail at once, but continues to develop cracks at loads up to about 2000 lbs/in. This gradual failure can be explained in part by a spatial variation of the value of Y, since the 8.2 ksi used is only an average value. A better explanation, though, is contained in a paper by Pagano [4], where he reports that the absorption of around 0.3 % moisture, by weight, by the composite will almost completely relax the thermal stresses. If these stresses are relaxed,

TABLE I

SUMMARY OF PROPERTIES* FOR AS-3501

Elastic Stiffness Properties	Tensile Value	Compressive Value
E_1	20.2×10^6 psi	17×10^6 psi
E_2	1.4×10^6 psi	1.6×10^6 psi
ν_{12}	0.28	0.28
G_{12}	0.65×10^6 psi	0.65×10^6 psi
Strength properties		
X	235,000 psi	180,000 psi
Y	8,200 psi	25,000 psi
S	17,900 psi	17,900 psi
Other properties		
Thermal expansion coefficients		
α_1 (fiber direction)	-0.2×10^{-6} in/in/^oF	
α_2 (transverse direction)	13×10^{-6} in/in/^oF	
Fiber volume fraction 0.62		
Ply thickness 0.0052 ± 0.0004 in		
Void content 2 %		
Density 0.057 lb/in^3		
Stress-free temperature 278^oF		

*Data supplied by Hercules, Inc.

TABLE II

THERMAL, MECHANICAL, AND TOTAL STRESSES, AND AVERAGE LAMINATE PROPERTIES AT FIRST PLY FAILURE IN TYPE I AND II LAMINATES

Layer Orientation	Stress Direction	Thermal Stress(ksi)	Mech. Stress(ksi)	Total Stress(ksi)
0^o	σ_1	-4.77	53.9	49.12
	σ_2	4.77	- 0.07	4.70
	τ_{12}	0	0	0
90^o	σ_1	-4.77	-15.17	-19.94
	σ_2	4.77	3.42	8.19
	τ_{12}	0	0	0
45^o	σ_1	-4.77	19.36	14.59
	σ_2	4.77	1.67	6.44
	τ_{12}	0	- 2.90	- 2.90
-45^o	σ_1	-4.77	19.36	14.59
	σ_2	4.77	1.67	6.44
	τ_{12}	0	2.90	2.90

$$E_{xx} = 8.11 \times 10^6 \text{ psi}$$
$$E_{yy} = 8.11 \times 10^6 \text{ psi}$$
$$V_{xy} = 0.299$$
$$G_{xy} = 3.12 \times 10^6 \text{ psi}$$

TABLE III

THERMAL, MECHANICAL, AND TOTAL INTERLAMINAR NORMAL STRESS AT FIRST PLY FAILURE IN TYPE I AND II LAMINATES

Interface	Thermal Stress(ksi)	Mech. Stress(ksi)	Total Stress(ksi)
Type I Laminate:			
0^o / 45^o	0.48	-.01	0.47
45^o / -45^o	1.44	0.74	2.18
-45^o / 90^o	2.40	3.02	5.42
90^o / 90^o	2.88	4.55	7.43
Type II Laminate:			
0^o / 90^o	0.48	-.01	0.47
90^o / 45^o	0.96	-1.55	-0.59
45^o / -45^o	0.96	-3.84	-2.88
-45^o / -45^o	0.96	-4.61	-3.65

the applied load necessary to cause failure of the 90^{o} layers increases to approximately 2000 lbs/in.

Another observation not explained by laminate theory, or the application of a failure criterion to the stresses predicted by laminate theory, is the almost regular spacing of the transverse cracks. Reifsnider [3] has addressed this problem by assuming that, in the region of the transverse cracks, the surrounding layers take up the load previously carried by the cracked lamina, and attempts to find at what distance away from the crack the stress in the failed layer recovers its original value. He then assumes that another crack will form at this distance, and thus predicts the crack spacing. For a type I laminate, he predicts a spacing of 0.029" in the 90^{o} layers, with observed spacings of $0.024^{"}$ - $0.059^{"}$. For a type II laminate, he predicts a spacing in the 90^{o} plies of $0.014^{"}$, with observed spacings ranging from $0.009^{"}$ to $0.017^{"}$. The observed spacings depend upon both the maximum load and the total number of cycles that the specimen undergoes, and decreases with both increasing load and increasing number of cycles.

One last observation worth noting is that the 90^{o} laminae in the type I material act, essentially, as one layer of twice the thickness. Hence, the transverse cracks in type I laminates would have a much wider opening than those in type II laminates, where the 90^{o} laminae are independent.

Once the 90^{o} laminae begin to fail, laminate theory is no longer applicable, and attempts to predict the failure of the 45^{o} laminae are somewhat dubious. Experimentally, the 45^{o} plies adjoining the 90^{o}

plies begin to develop transverse cracks shortly after their development in the 90^{o} layers, and the damage progresses throughout the interior of the laminate.

The existence of the second type of damage is predicted by the Pipes-Pagano σ_z approximation. Due to the stacking sequence, very high tensile stresses are present between the layers of the type I laminate, while the stresses are predominantly compressive in the type II laminates. This is evidenced by extensive delaminations along the edges of type I specimens. Occasionally, the type II specimens delaminate near the end tabs, but this appears to be a grip related phenomenon. Little work has been done to date to determine the depth of the delamination as a function of load or number of fatigue cycles, but it appears to extend at least a quarter of an inch into the width, at or near specimen fracture, of a 1" wide specimen.

As specimens of either material are loaded in simple tension, the stress-strain curve becomes bilinear at loads of approximately 2000 lbs/in. This knee, though not evident in all specimens, is probably related to the amount of transverse cracking in the various layers. The predicted change in E_{xx} with complete failure of the 90^{o} layers is about 4 %, while if all the interior layers fail, the change is about 22 %. The actual values found range from about 6 % to 18 %, indicating that the knee is some combination of failure in the 90^{o} plies as well as in the 45^{o} plies. The knee in type II laminates is generally more gradual than in type I, for unexplained reasons.

4. WAVES IN SOLIDS

Wave propagation in all materials is governed by the equation of motion:

$$\sigma_{ij,j} = \rho \ddot{u}_i \quad . \tag{19}$$

If the material in question is linear elastic, homogeneous, and isotropic, the stresses can be replaced with spatial derivatives of the displacements, u_i, and the Lame constants, λ and μ, to obtain

$$(\lambda + \mu)\, u_{j,ji} + \mu u_{i,jj} = \rho \ddot{u}_i \quad . \tag{20}$$

Generally, a wave is considered to have a sinusoidal time variation, and complex notation is used. It must be remembered, in what follows, that the actual wave is mathematically described by the real part (real part convention) of the complex wave function. Thus u_i is represented by a time varying portion, e^{-iwt}, multiplied by a spatially varying portion, $\bar{u}_i$. The time portion of Eqn. (20) is then eliminated, and the remaining partial differential equation is solved by appropriate means.

Three of the most commonly discussed waves which can propagate in a solid are the longitudinal plane and spherical waves, and a transverse plane wave. A mathematical description of any plane wave is

$$u_j = A_j e^{i(Kn_\ell X_\ell - wt)} \tag{21}$$

where n_ℓ are the components of the unit vector normal to the wave front; w is the angular frequency of the wave; and k is the wave number. Numerically, k is equal to the ratio of the angular

frequency to the appropriate wave speed, while the longitudinal and transverse wave speeds, V_L and V_T respectively, are given by

$$V_L = \left(\frac{\lambda + 2\mu}{\rho}\right)^{1/2}$$
$$V_T = \left(\frac{\mu}{\rho}\right)^{1/2} \tag{22}$$

If Eqn. (20) is solved in spherical coordinates, with u_r being the only non-zero displacement and all quantities being independent of angular orientation, then a longitudinal spherical wave can be found which propagates with displacements given by

$$u_r = Ak \left(\frac{1}{kr} + \frac{i}{k^2 r^2}\right) e^{i(kr - \omega t)} \tag{23}$$

where r is the distance to a field point from the source of the spherical wave, and k is the longitudinal wave number. For both kinds of longitudinal waves, the particle displacements are always parallel to the wave front normal, while for transverse waves, the displacements are perpendicular to the wave front normal.

Equations (21) and (23) are mathematical descriptions of waves in ideal materials, but all real materials absorb some of the energy carried by the wave as it travels through the medium. This absorption process is called attenuation, and is usually described mathematically by allowing the wave number to become complex; i.e.,

$$\bar{k} = k + i\alpha \tag{24}$$

with k being the usual wave number and α the amplitude attenuation coefficient. Eqns. (21) and (23) then become

$$u_j = A_j e^{-\alpha n_\ell x_\ell} e^{i(kn_\ell x_\ell - wt)} \tag{25}$$

$$u_r = Ake^{-\alpha r} e^{i(kr - wt)} \left(\frac{1}{kr} + \frac{i}{k^2 r^2}\right) \tag{26}$$

The attenuation coefficient is a function of many things, among which are: the material serving as a sound medium, the frequency w, and the damage or material discontinuities existant in the material. Hence, it is generally possible to obtain a measure of the amount of damage introduced into a material by external forces by measuring the change in attenuation.

This coefficient is usually measured by a technique called the pulse-echo method. An ultrasonic transducer is fastened to one surface of a block of material by some bonding agent, usually a thin grease such as glycerin. The transducer is electrically coupled to a pulse generator-receiver which emits high energy bursts, or pulses, of very high frequency (2 - 50 MHz) and short duration (2 - 5 μsec). These electrical pulses are converted to mechanical vibrations (sound) of the same frequency by the transducer. The sound pulses then travel through the material and reflect off of the opposite surface, returning to the transducer and causing it to vibrate. A portion of the mechanical energy of the transducer is converted back into electrical energy which passes to the receiver and is displayed upon a CRT as an echo. The reflections continue until they eventually die out, resulting in a series of echoes on the CRT. An examination of the maximum

amplitude in each echo will yield the attenuation coefficient.

Suppose that the block being tested is of length L. Then the distance traveled by each echo is 2nL, where n is the number of the echo. Suppose also that the wave travelling in the material can be adequately described by Eqn. (25). The maximum amplitude of the n^{th} echo is then given by

$$u_n = A_o e^{-2n\alpha L} \tag{27}$$

with A_o being the initial amplitude of the sound wave. If the ratio of u_m to u_n is taken, with n being greater than m, one obtains

$$\frac{u_m}{u_n} = e^{2\alpha(n-m)L} \tag{28}$$

Hence, the attenuation coefficient is found to be

$$\alpha = \frac{1}{2L(n-m)} \ln \frac{u_m}{u_n} \tag{29}$$

with units of nepers/cm.

The length of the specimen is important because the pulse must be shorter than the time required for an echo to return. If not, the returning echoes interfere with the original pulse, as well as with each other, making the determination of the maximum amplitude either incorrect or impossible. As discussed by Truell [5], other factors can also affect the accuracy of attenuation measurements. Foremost among these are losses which occur because of the coupling agent, losses resulting from non-parallelness of the two reflecting surfaces

of the specimen, and losses associated with the diffraction of the sound wave as it leaves the circular transducer. Some, or most, of these errors can be accounted for, as will be discussed later.

Units other than nepers/cm. are often used to describe attenuation. Two of the most common are decibels per inch (dB/in) and decibels per echo (dB/echo). They are defined as

$$\alpha = \frac{20}{2L(n-m)} \log_{10} \frac{u_m}{u_n} \tag{30}$$

and

$$\alpha = \frac{20}{(n-m)} \log_{10} \frac{u_m}{u_n} \tag{31}$$

Unless otherwise specified, units of dB/echo will be used in what follows.

It is unfortunate that most composite specimens are not very thick; the usual eight-ply laminate has a time between echoes of about 1 μsec, while the minimum pulse width achievable with presently existing equipment at VPI & SU is between 1-1/2 to 2 μsec. For this reason, a fused silica delay block is used to obtain a larger time separation between echoes.

Several reports ([6], [7]) have been made concerning the use of buffer blocks in making attenuation measurements. Papadakis' technique [6], though very useful on thin specimens, places severe restrictions on equipment performance which the presently used system is not able to meet; one in particular is the requirement of a very fast-rising pulse. Reference [7] relaxes these requirements, but in order to do so,

places a lower limit on the number of plies in the laminate at about fifteen. Both techniques placed the buffer block between the specimen and transducer, and kept track of the multiple reflections which occur at the buffer block-specimen interface. After thoroughly exploring the above techniques, they were discarded as being useless for composite specimens of eight plies or less, at the present time.

Another technique which also has been tried at Virginia Tech consists of reversing the locations of the specimen and buffer block. A picture of the transducer and buffer block mounted on a specimen is shown in Fig. 2. The c-clamp is used to hold the three objects together as the specimen is being loaded in tension or fatigue. Figure 3 is a photograph of a typical oscilloscope trace using this arrangement. Note that the echo train consists of several large echoes (major echoes) evenly spaced, with a series of smaller echoes (minor echoes) trailing each major echo. These minor echoes return so closely to the major echoes as to be individually indistinguishable; hence, only the major echoes can be used to obtain any useful information. Figure 4 is a schematic diagram which shows the paths taken by the first two major echoes. The paths taken by the minor echoes have been omitted for clarity. These major echoes correspond to the portion of the wave which passes completely through the specimen and into the buffer block, after which it simply reflects back and forth in the buffer block, releasing a portion of its energy into the specimen at each reflection at the buffer block-specimen interface. It is this last portion of the wave which reaches the transducer and is shown on the

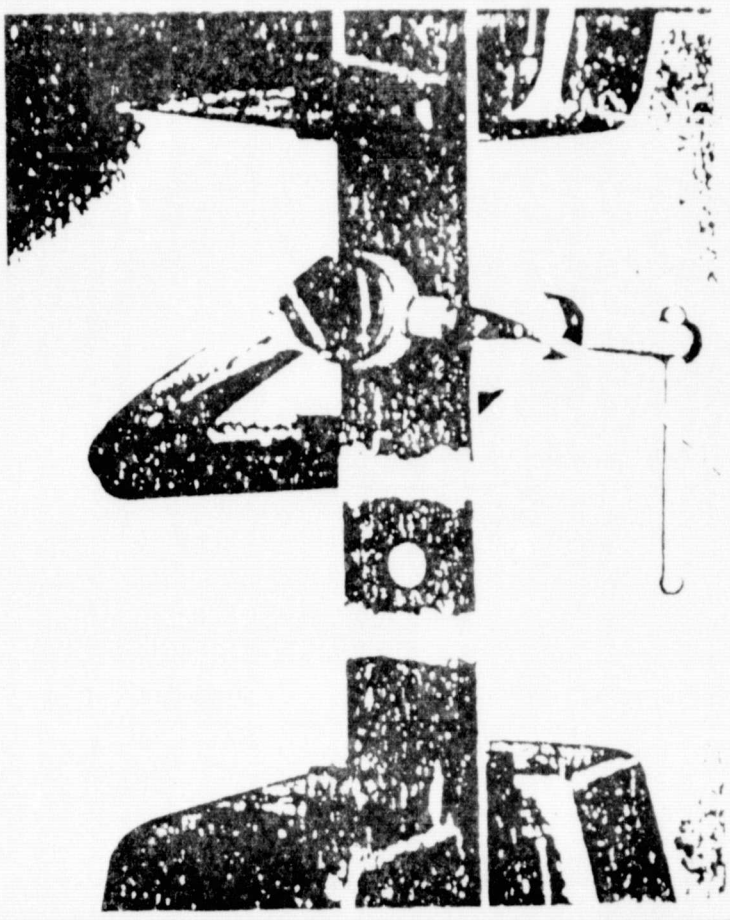

Figure 2. Photograph of the Delay Block and Transducer Mounted to a Specimen

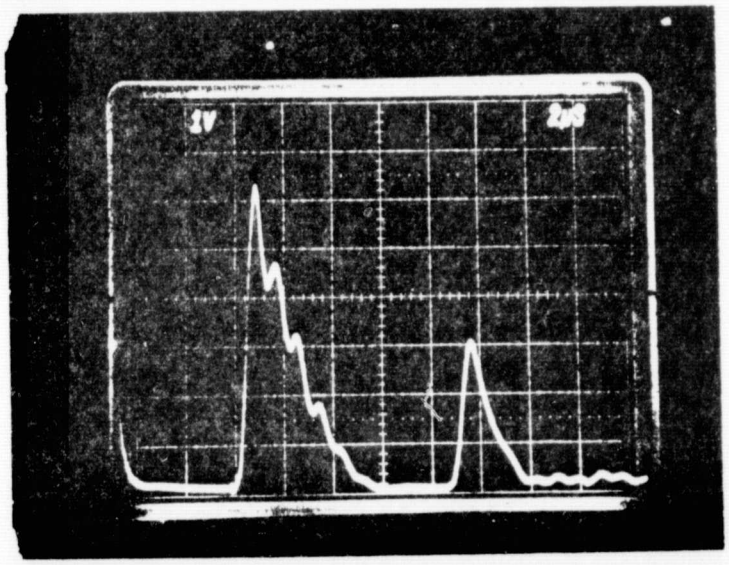

Figure 3. Typical Oscilloscope Trace for the Transducer - Specimen - Delay Block Combination

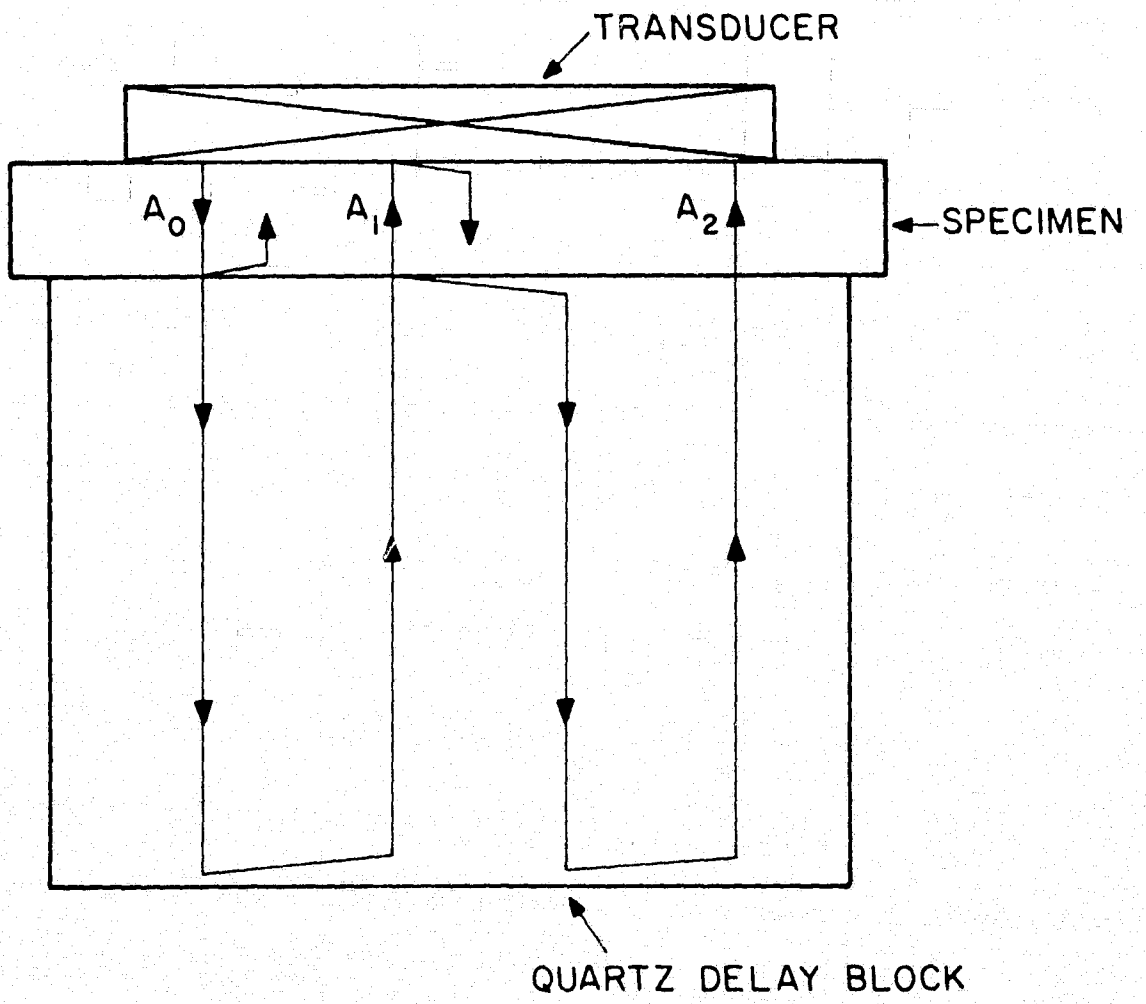

Figure 4

Schematic Representation of the First and Second Major Echoes

CRT as a major echo.

To obtain a good estimate of the relative amplitudes of the first two major echoes, assume that a plane wave is emitted from the transducer. Let α_1 and α_3 be the amplitude attenuation coefficients of the specimen and buffer block, respectively, in units of decibels per round trip in either. As shown by Hayford [7], the maximum amplitude of a wave reflected from a bond between two materials is a reflection coefficient, R, times the maximum amplitude of the wave incident upon the interface. The transmitted portion is treated similarly, with its magnitude being equal to a transmission coefficient, T, times the incident amplitude. Since, in general, the side of the interface from which the wave is incident is important, both R and T will be given two subscripts. The first denotes the incident material. The second denotes the material on the other side of the interface; thus, R_{13} denotes the reflection coefficient of the wave incident upon the 1-3 interface, from material 1. A schematic representation of the necessary reflection and transmission coefficients is shown in Fig. 5. From [7]

$$T_{31} = \frac{4z_2z_3}{(z_1 + z_2)(z_2 + z_3)e^{-i\beta\ell} + (z_2 - z_3)(z_1 - z_2)e^{i\beta\ell}} \tag{32}$$

$$R_{31} = \frac{(z_3 - z_2)(z_1 + z_2)e^{-i\beta\ell} + (z_2 + z_3)(z_2 - z_1)e^{i\beta\ell}}{(z_3 + z_2)(z_1 + z_2)e^{-i\beta\ell} + (z_2 - z_3)(z_1 - z_2)e^{i\beta\ell}} \tag{33}$$

with β being the wave number in the bonding agent, and ℓ the bond thickness. The acoustic impedance, z, of a material is given by the

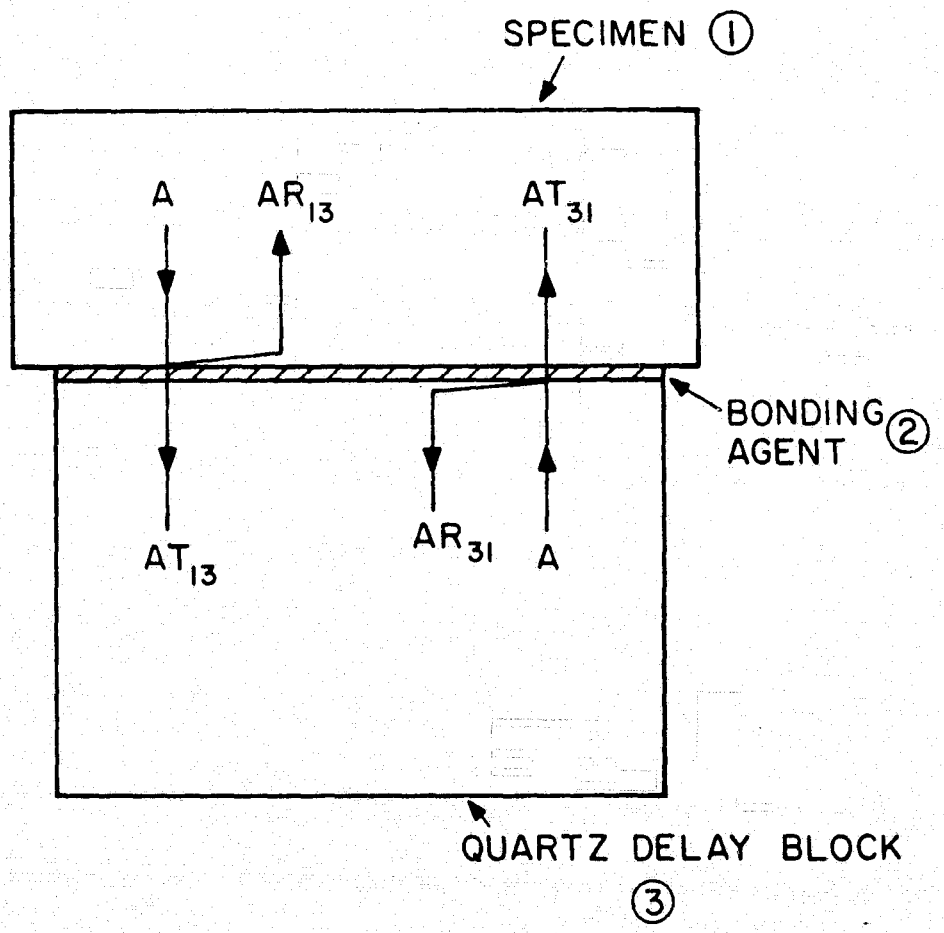

Figure 5

Schematic Representation of the Transmission and Reflection Coefficients

product of the wave speed and density. The transmission and reflection coefficients T_{13} and R_{13} can be obtained by interchanging z_1 and z_3 in Eqns. (32) and (33), respectively. Note that the coefficients are complex, indicating the possibility of a phase shift other than zero or pi, which is the case for an interface between only two materials.

An analysis of the schematic representation of Fig. 4 is now given. In what follows, the word "amplitude" shall refer to the maximum amplitude of an echo. Assume that the amplitude of the wave just after leaving the transducer is given by A_o. This wave travels through the specimen until it reaches the interface, at which point it has an amplitude of $A_o 10^{-\alpha_1/40}$. The portion that is transmitted is the only part of interest, and just on the other side of the interface, its amplitude is $A_o T_{13} 10^{-\alpha_1/40}$. The wave travels through the delay block until it strikes the lower end, where it completely reflects. When it again reaches the interface, the amplitude is $A_o T_{13} 10^{-\alpha_1/40-\alpha_3/20}$. Now this wave breaks into two parts. One portion is transmitted across the bond and travels through the specimen to the transducer, introducing a T_{31} and another $10^{-\alpha_1/40}$. Thus A_1, the amplitude of the first major echo, is given by

$$A_1 = A_o |T_{13} T_{31}| 10^{-\alpha_1/20-\alpha_3/20} \tag{34}$$

Continuing in the above manner and following the above-mentioned portion which reflects at the interface, it is found that A_2, the amplitude of the second major echo, is given by

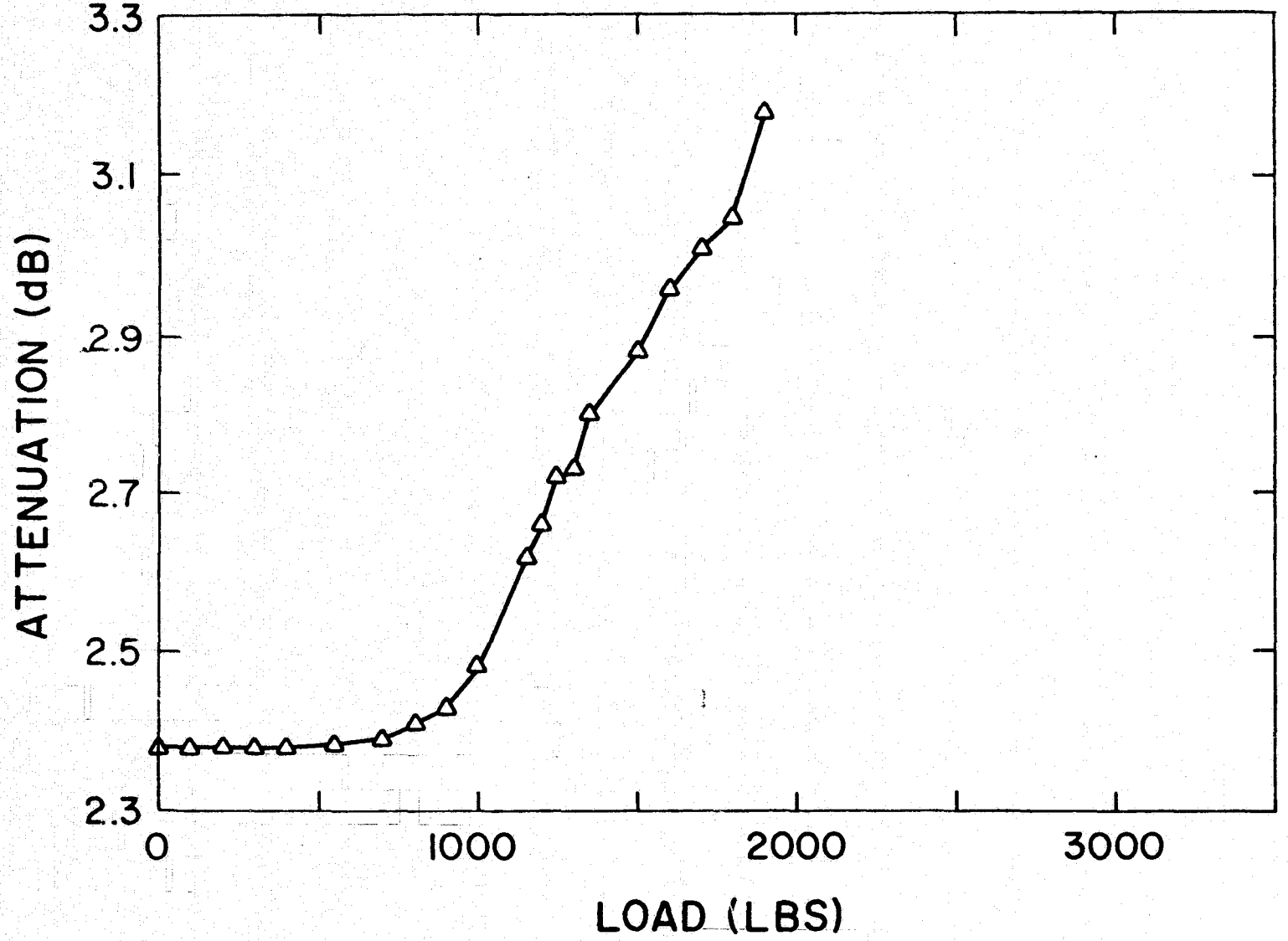

Fig. 6 Attenuation vs. Load for Specimen D-5 (Type I)

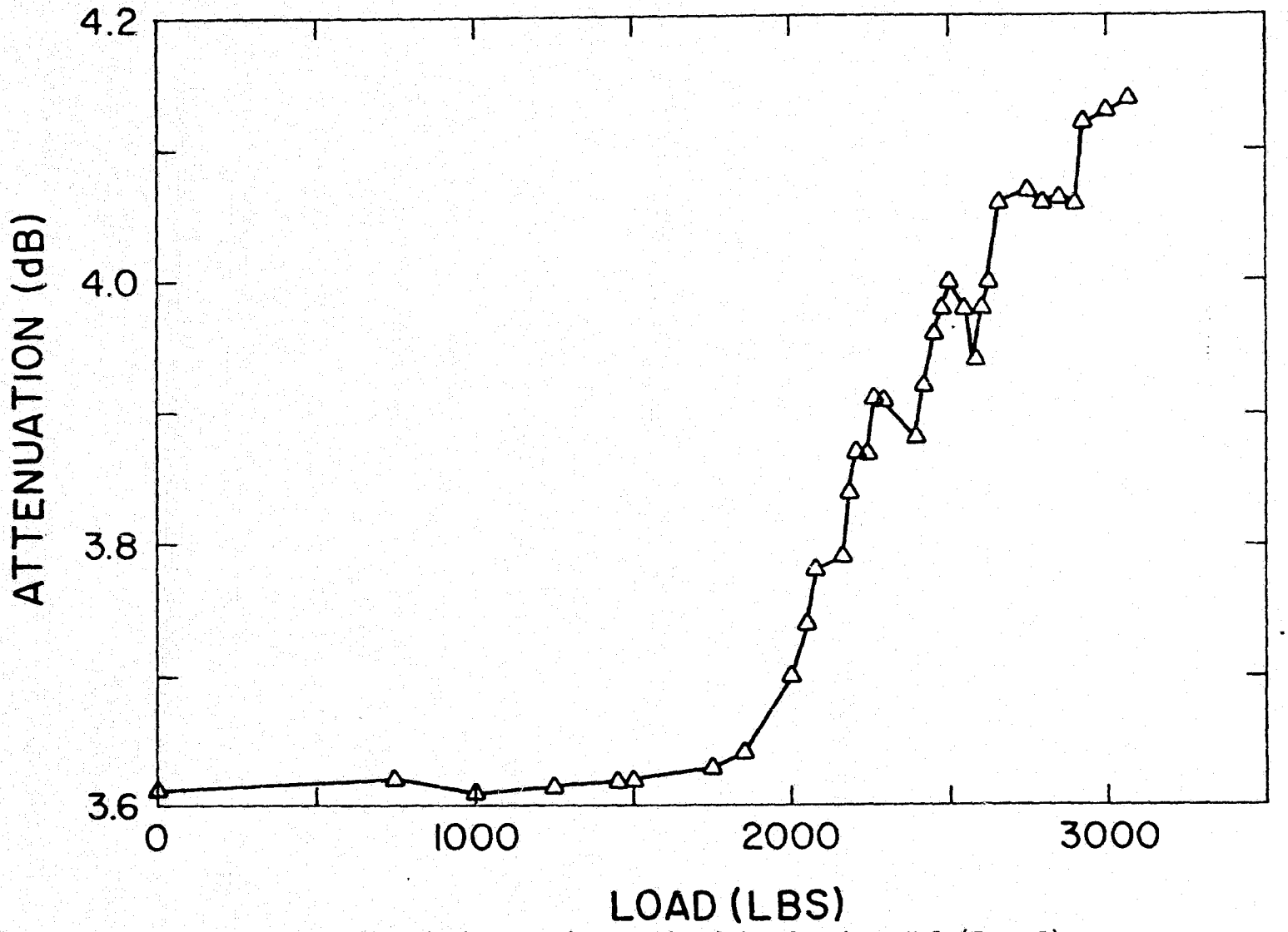

Fig. 7 Attenuation vs. Load for Specimen X-1 (Type I)

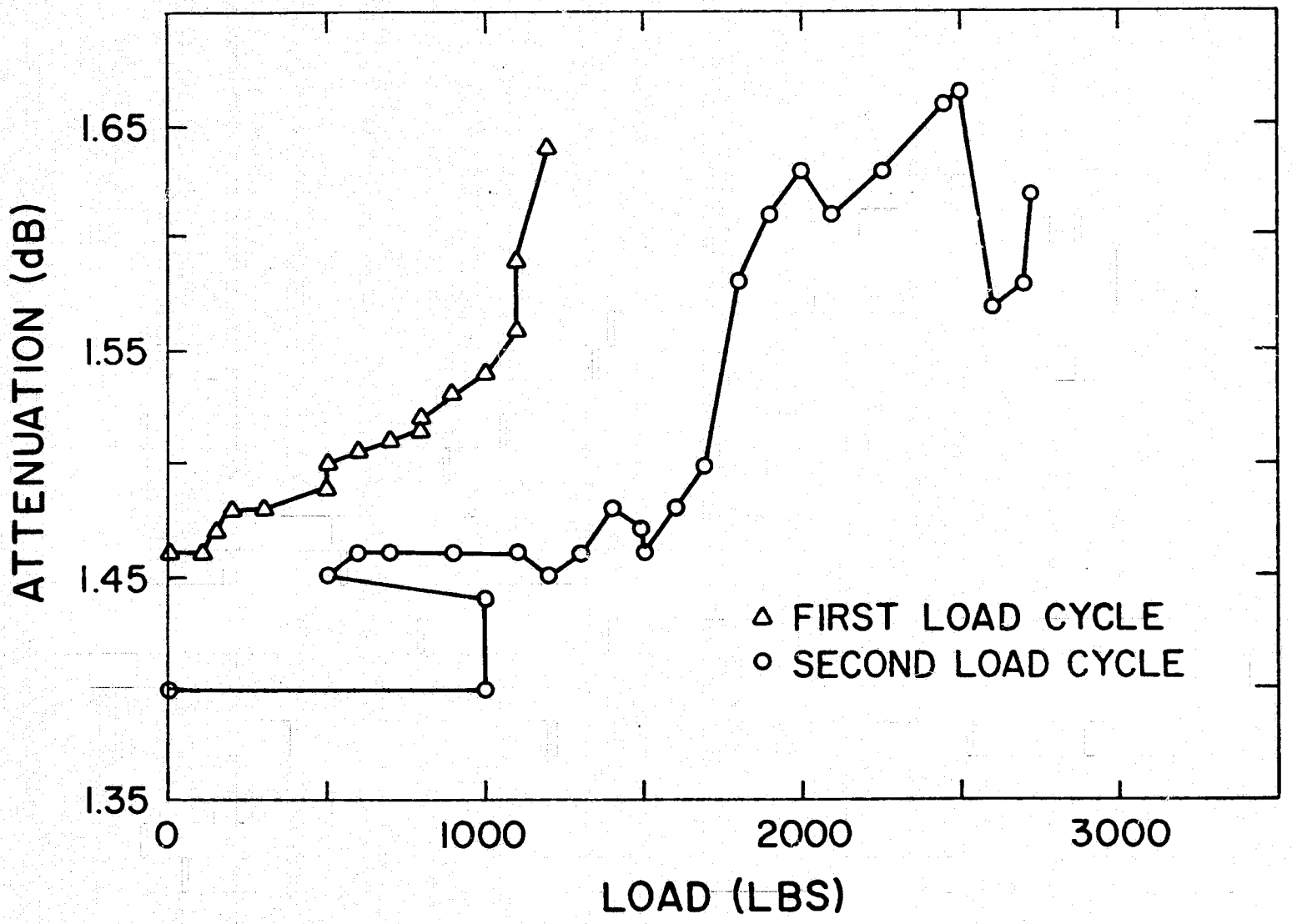

Fig. 8 Attenuation vs. Load for Specimen D-6 (Type I)

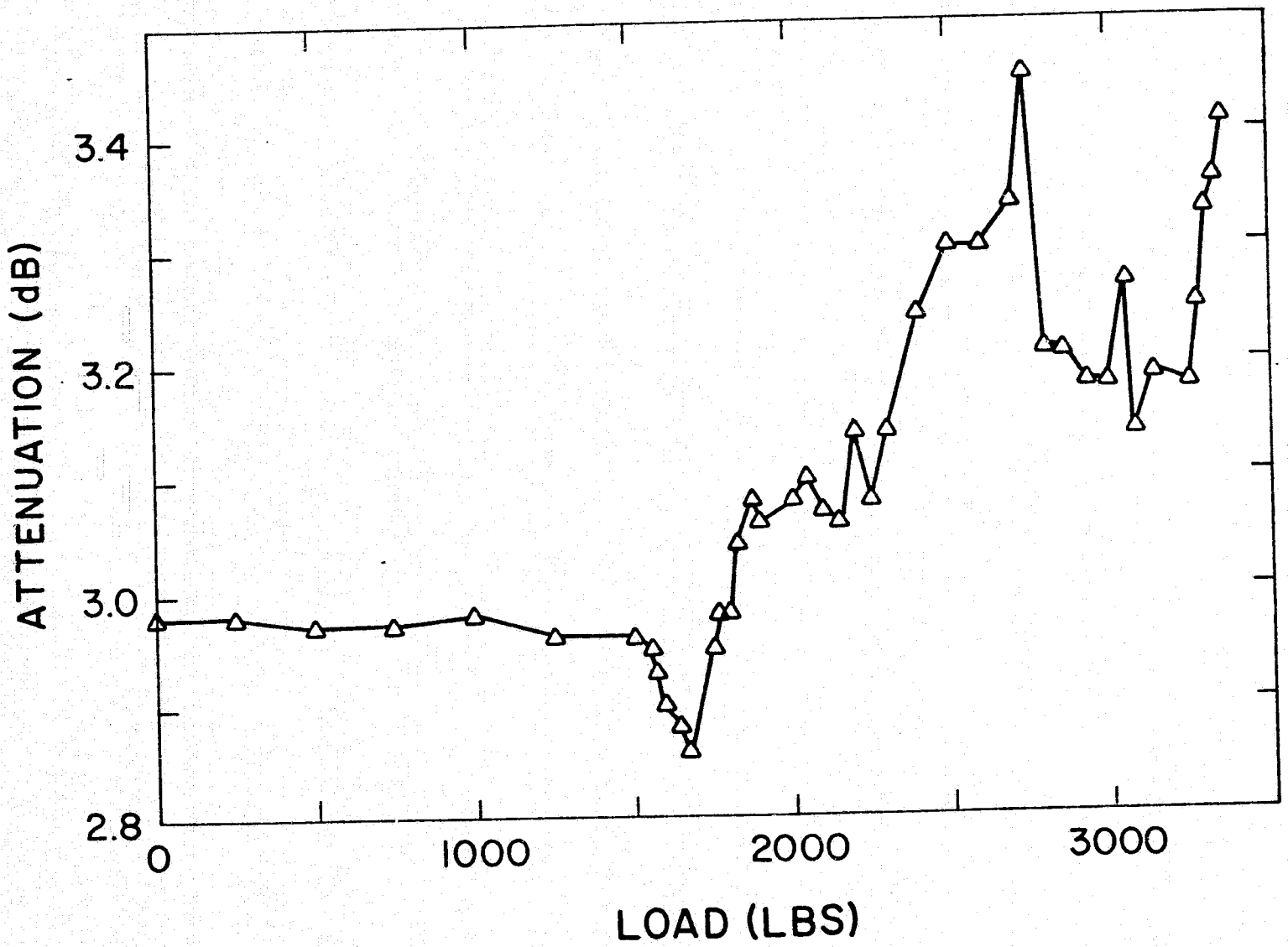

Fig. 9 Attenuation vs. Load for Specimen 2624-18 (Type II)

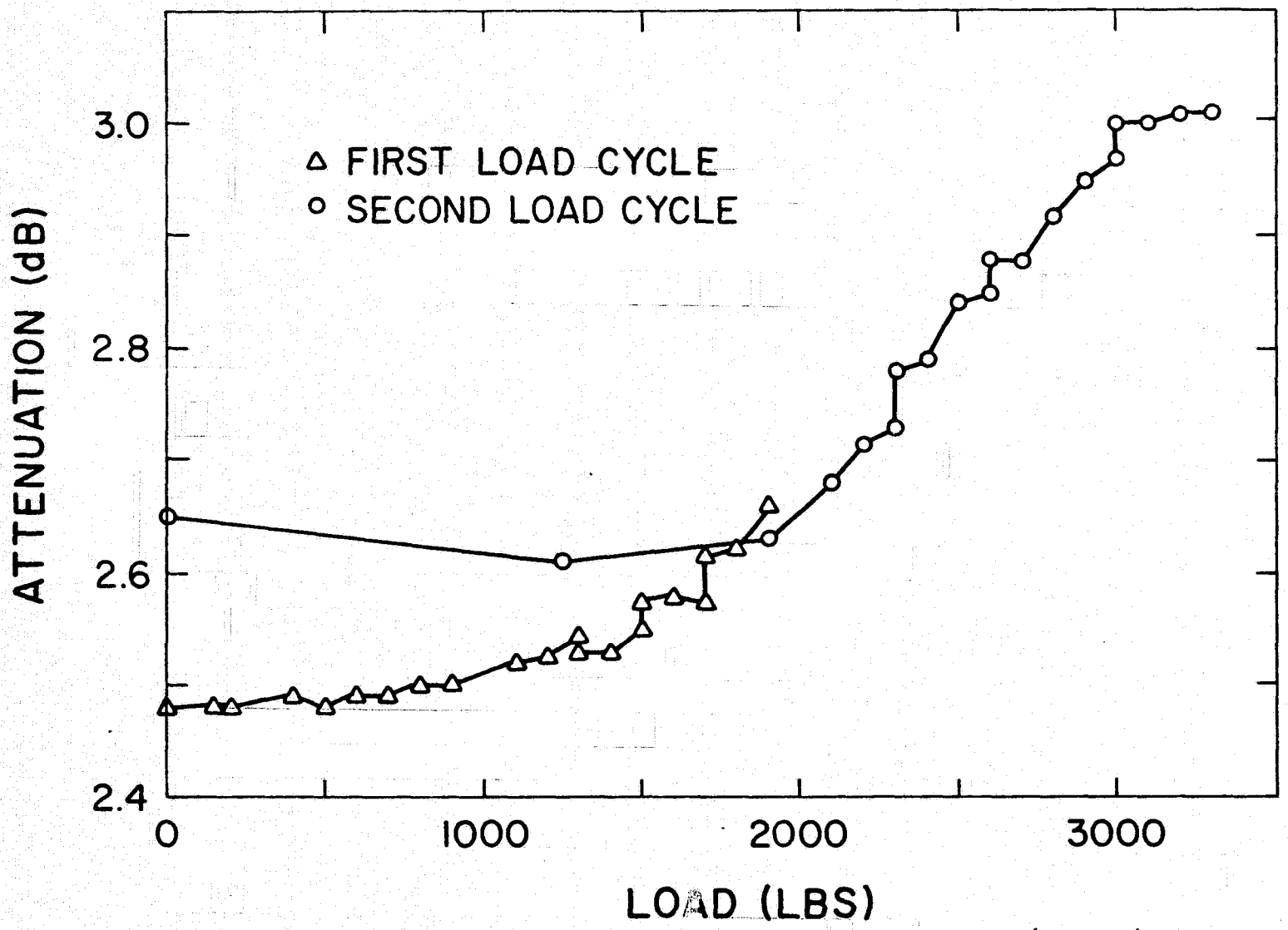

Fig. 10 Attenuation vs. Load for Specimen 2626-10 (Type II)

$$A_2 = A_o|T_{13}T_{31}R_{31}|10^{-\alpha_1/20-\alpha_3/10} \tag{35}$$

If Eqn. (31) is now used to find the loss in dB/echo, one obtains

$$\alpha = \alpha_3 - 20 \log |R_{31}| \tag{36}$$

Thus, as is seen in the above analysis, the only information which appears to be contained in the major echoes is the attenuation of the quartz buffer and the magnitude of the reflection coefficient, R_{31}.

Tests of this nature have been conducted on specimens undergoing quasi-static tension, and significant changes, which are either positive or negative, have been observed at load resultants ranging from 1000 to 2000 lbs/in, as shown in Figs. 6 through 10, for both type I and type II specimens. It is interesting to note that these changes are not monotonic and can be either gradual or very sudden. Note also that the above load ranges span the values at which the 90^o layers are predicted to fail, and at which delaminations are observed to form. Obviously, these rises have nothing to do with changes in α_3, since no loads are applied to the quartz delay block. It appears, then, from Eqn. (36), that the change in attenuation must occur because of changes in the bond (more specifically, the bond thickness), since there is no other quantity which could change during loading in this equation. That possibility will now be investigated.

From Eqn. (33), the magnitude of R_{31} is

$$|R_{31}| = \left[\frac{-2z_1z_2^2z_3 + \cos^2\beta\ell(z_1^2 + z_3^2)z_2^2 + \sin^2\beta\ell(z_2^4 + z_1^2z_3^2)}{2z_1z_2^2z_3 + \cos^2\beta\ell(z_1^2 + z_3^2)z_2^2 + \sin^2\beta\ell(z_2^4 + z_1^2z_3^2)} \right]^{1/2} \quad (37)$$

while the values of z_1, z_2, and z_3 are

$$\begin{aligned} z_1 &= 4000 \text{ g/cm}^2\text{-sec} \\ z_2 &= 2400 \text{ g/cm}^2\text{-sec} \\ z_3 &= 13000 \text{ g/cm}^2\text{-sec} \end{aligned} \quad (38)$$

Figure 11 shows a plot of both $|R_{31}|$ and the bond loss term, $-20 \log |R_{31}|$, as a function of $\beta\ell$. Note that $|R_{31}|$ has a maximum at $\beta\ell$ equal to $\pi/2$, resulting in a minimum in the bond loss. This minimum is calculated to be 1.9 dB. Returning to Eqn. (36), a minimum value of α is actually a function of two variables, α_3 and R_{31}. However, fused silica is used as a buffer material precisely because of its very low intrinsic attenuation. Hence, it is reasonable to assume that the minimum value of α occurs at the minimum value of $-20 \log |R_{31}|$. At this point, $\beta\ell$ equals $\pi/2$. Recalling the definition of the wave number, it is found that

$$\frac{2\pi f\ell}{V_b} = \frac{\pi}{2} \quad (39)$$

where f is the frequency of minimum attenuation, and V_b is the velocity of sound in the bond. For glycerin, this latter value is approximately 2500 m/sec. Hence, the bond thickness, in inches, is given by

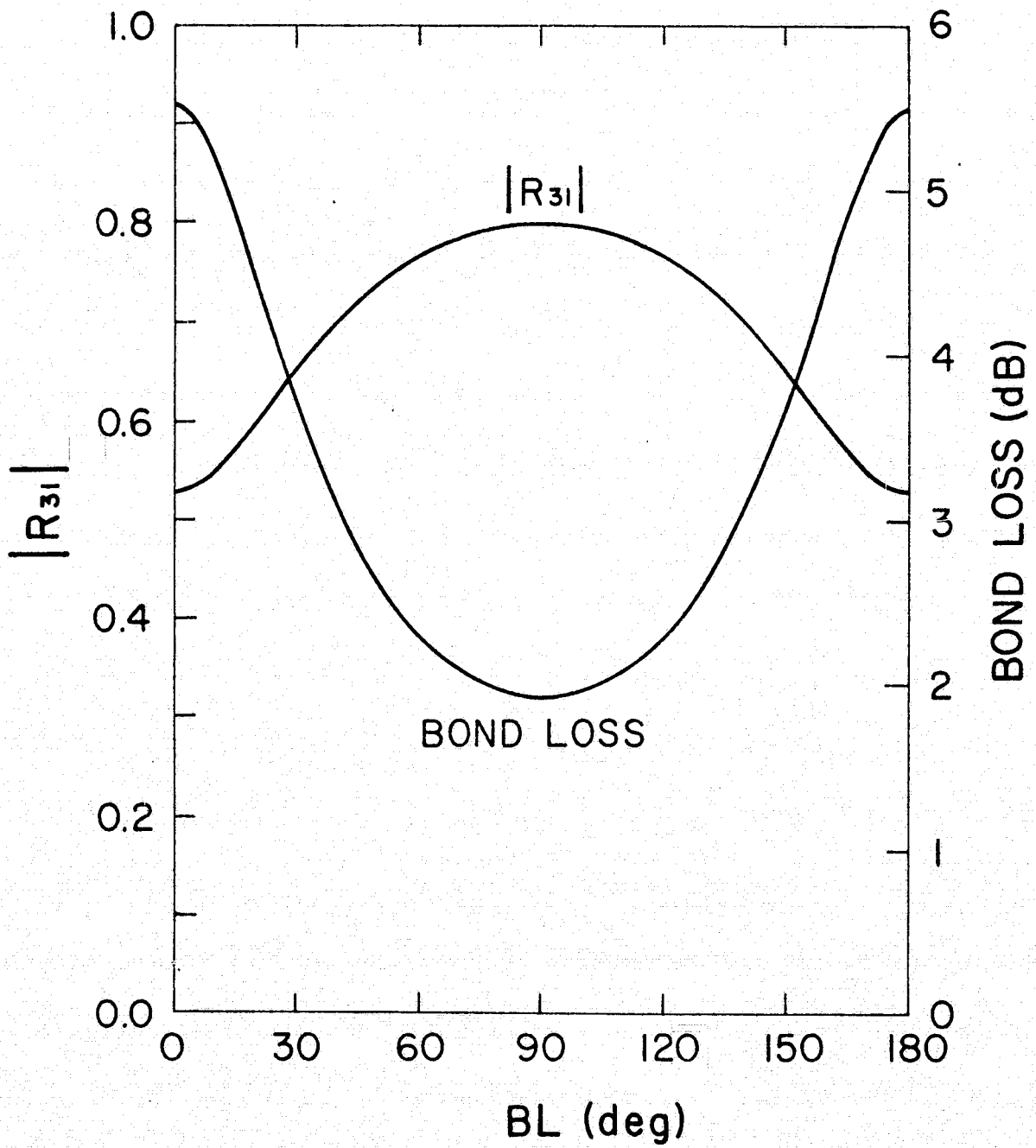

Fig. 11 The Reflection Coefficient and the Bond Loss as a function of $\beta\ell$

$$\ell = \frac{24600}{f} \tag{40}$$

A specimen was loaded in tension to 2100 lbs., and values of the frequency at minimum attenuation were recorded at approximately 200 lb. increments. At zero load, this frequency was 25.5 MHz, and at 2000 lbs., it was 24.4 MHz, corresponding to an initial bond thickness of .00096 in. and increasing to .00101 in., a change of .00005 in. If the frequency is reduced to the normal testing frequency of 5 MHz, the bond losses would then become 4.7 dB and 4.6 dB, respectively, indicating a decrease in attenuation of 0.1 dB over the range of the test. Of course, these values are only approximate for other tests, but they are reasonable estimates based upon the above assumptions. The important thing, however, is not the actual values, but the tendency of the bond to become thicker as the specimen thickness decreases when loaded. The bond thickness is always close to .001 in., and at this thickness, the attenuation due to bond losses will always decrease with increasing load. Thus, it is hardly likely that bond losses can account for the large (1 to 2 dB) increases found in the tests run.

While making attenuation measurements with high accuracy, experimentalists often make what could be called second-order corrections. These second-order losses, usually less than one decibel, are generally of a lesser magnitude than primary losses, such as the bond loss described above. Among these second-order losses are those which occur in the transducer, and those due to the diffraction exhibited by any finite-sized wave source, such as a transducer. The former, since

it is not affected by loads which occur in the specimen, will be ignored, and a correction term will be added to Eqn. (36) to express the diffraction losses. Thus

$$\alpha = \alpha_3 - 20 \log |R_{31}| + \alpha_D \tag{41}$$

where α_D is the, as yet unspecified, diffraction loss.

In the study of optical diffraction, three main types of diffraction effects are discussed. They are diffraction by single- and multiple-slit gratings, and diffraction by sharp edges. Sound waves will behave similarly, and it is readily apparent that both transverse cracks and delaminations in a specimen could serve to act as these types of diffraction gratings for ultrasonic waves of appropriate wavelengths. Thus, a short presentation of the theory of diffraction is in order, and is presented in the next section.

5. ULTRASONIC DIFFRACTION THEORY

In order to find a mathematical description of a sound wave after it has passed through some aperture, one need only apply the equations of elasticity, together with appropriate boundary conditions, and solve. Unfortunately, the mathematics involved has not seen fit to cooperate with the theoretician, necessitating the use of simpler equations. The theory of light diffraction has been well explored (see, for example, [8], [9]), and the equations derived for the scalar diffraction of light can be easily adapted to the diffraction of ultrasonic waves in certain media; notably, compressible, inviscid fluids. The term scalar diffraction is used for those cases where the vectorial aspect of light waves is insignificant.

The use of a fluid medium to study diffraction effects in solids has been justified by several researchers. Truell [5] and Papadakis [10] have both done considerable research on diffraction effects in velocity and attenuation measurements in solids using a fluid medium for their theoretical calculations. Both showed excellent agreement between theory and experiment. Papadakis also modified the wave number, k, to account for the anisotropy of crystalline solids while still assuming a fluid medium, and achieved good agreement between theory and experiment.

Wave motion in fluids is similar, in some respects, to that in solids, and is also governed by the equation of motion, Eqn. (19). But Eqn. (20) is simplified because, for inviscid fluids, the Lame constant μ is zero. Thus Eqn. (20) becomes

$$\lambda u_{j,ji} = \rho \ddot{u}_i \tag{42}$$

By taking one more derivative with respect to the spatial coordinate x_i, one obtains

$$\lambda u_{j,jii} = \rho \ddot{u}_{i,i} \tag{43}$$

The dilatation Δ is defined as $u_{i,i}$. Hence

$$\lambda \nabla^2 \Delta = \rho \ddot{\Delta} \tag{44}$$

If the dilatation is assumed to have a sinusoidal time variation, one obtains Helmholtz's time-independent wave equation

$$(\nabla^2 + k^2)\Delta = 0 \tag{45}$$

with k being the usual wave number, and the velocity of sound being

$$V_L = \left(\frac{\lambda}{\rho}\right)^{1/2} \tag{46}$$

Lambda is usually replaced by B, the bulk modulus, in fluids. For solids, B is given by

$$B = \lambda + \frac{2}{3}\mu \tag{47}$$

while for fluids, B and λ are the same, since μ is zero.

The normal Hooke's Law for solids is modified slightly for fluids. Instead of relating strain to stress, the dilatation is related to the hydrostatic pressure, p, by the bulk modulus, to give

$$p = -B\Delta \tag{48}$$

and if B is independent of position, Eqn. (45) becomes

$$(\nabla^2 + k^2)p = 0 \tag{49}$$

To make the transition from solids to fluids complete, it is necessary to define attenuation in terms of a decrease in the dilatation, rather than in the displacement. The attenuation coefficient α is then

$$\alpha = \frac{1}{x_2 - x_1} \ln \frac{\Delta_1}{\Delta_2} \tag{50}$$

in units of nepers/cm., where Δ_1 and Δ_2 are the maximum dilatations at distances x_1 and x_2, respectively. Since the dilatation is proportional to the pressure, Eqn. (50) is also written

$$\alpha = \frac{1}{x_2 - x_1} \ln \frac{p_1}{p_2} \tag{51}$$

The other definitions of attenuation, Eqns. (30) and (31) are adjusted accordingly.

Kirchoff's diffraction integral ([7], [8]) was derived for scalar light waves, but can easily be adapted to sound waves in fluids. There are several methods for approaching this problem; the following is based upon the presentation of Sommerfeld [8].

Assume that some monochromatic sound disturbance, henceforth denoted by v, exists in a region of space V. By Green's theorem

$$\int_V (u\nabla^2 v - v\nabla^2 u)dV = \int_S (u \frac{\partial v}{\partial n} - v \frac{\partial u}{\partial n})dS \tag{52}$$

as long as u and v are suitably continuous functions. S is the

surface surrounding V, and $\frac{\partial u}{\partial n}$ is given by the dot product of $\vec{n}$ and the gradient of u, with $\vec{n}$ being the outward normal to S. All derivatives up to the second must exist for both u and v everywhere inside and on S.

Since v is a wave variable, such as pressure or dilatation, it must satisfy Helmholtz's equation

$$\nabla^2 v = -k^2 v \tag{53}$$

Suppose that u is also from the class of functions which satisfy Helmholtz's equation. Then the left-hand side of Eqn. (52) is identically zero, and one obtains

$$\int_S (u \frac{\partial v}{\partial n} - v \frac{\partial u}{\partial n}) dS = 0 \tag{54}$$

Let u be the function

$$u = \frac{e^{ikr}}{r} \tag{55}$$

where r is the distance from some point Q inside of S to any other point in or on S. Since u has a singularity at the point Q, a volume surrounding Q must be excluded from V. This is done by enclosing Q with a small sphere of radius ε, whose surface is denoted by S'. The entire volume, along with the various surfaces and normals, is shown in Fig. 12. For this choice of u, Eqn. (54) becomes

$$\int_{S+S'} (\frac{e^{ikr}}{r} \frac{\partial v}{\partial n} - v \frac{\partial}{\partial n} \frac{e^{ikr}}{r}) dS = 0 \tag{56}$$

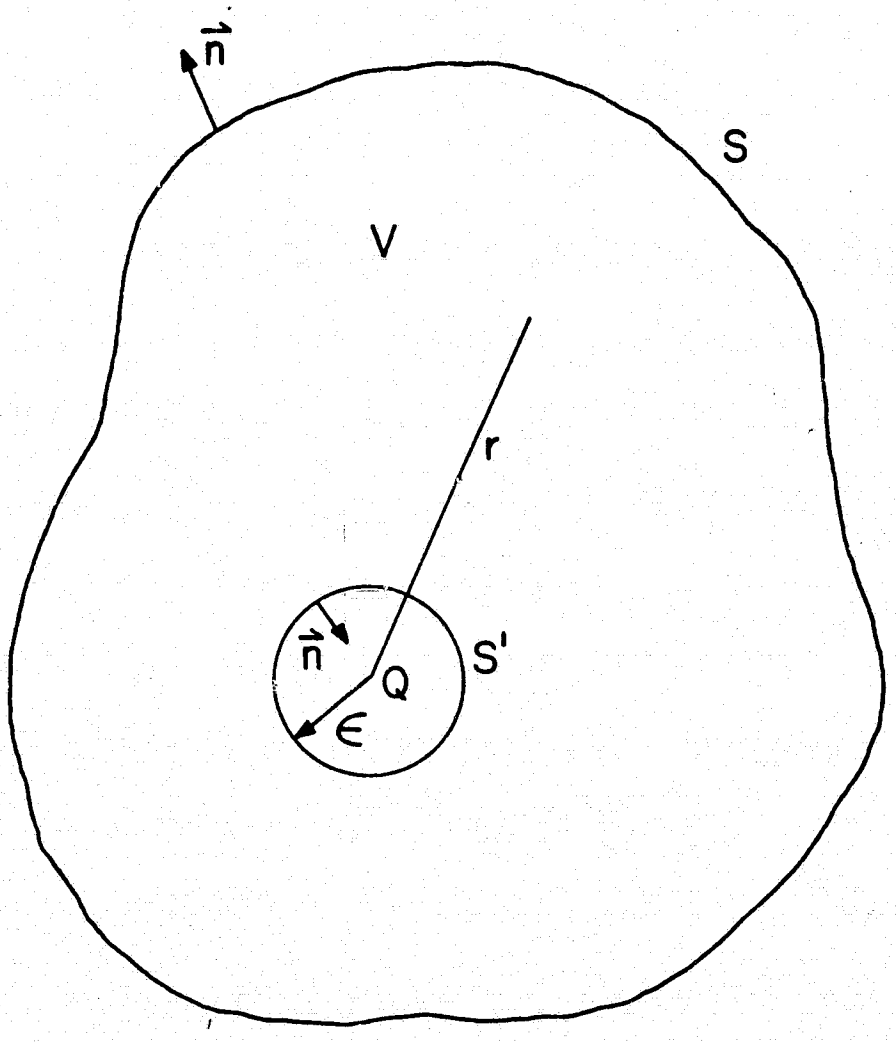

Figure 12

Region of Integration for Green's Theorem

or

$$\int_S \left(\frac{e^{ikr}}{r}\frac{\partial v}{\partial n} - v\frac{\partial}{\partial n}\frac{e^{ikr}}{r}\right)dS = \int_{S'} \left(v\frac{\partial}{\partial n}\frac{e^{ikr}}{r} - \frac{e^{ikr}}{r}\frac{\partial v}{\partial n}\right)dS \qquad (57)$$

On S', $\frac{\partial}{\partial n} = -\frac{\partial}{\partial r}$, and since $r = \varepsilon$ on S', Eqn. (57) becomes

$$\int_S \left(\frac{e^{ikr}}{r}\frac{\partial v}{\partial n} - v\frac{\partial}{\partial n}\frac{e^{ikr}}{r}\right)dS = \int_{S'} \left[\frac{e^{ik\varepsilon}}{\varepsilon}\frac{\partial v}{\partial r} - v\frac{e^{ik\varepsilon}}{\varepsilon}\left(ik - \frac{1}{\varepsilon}\right)\right]dS \qquad (58)$$

Because S' is a sphere, dS can be written as

$$dS = \varepsilon^2 d\Omega \qquad (59)$$

where Ω is the solid angle describing the sphere. Equation (58) then becomes

$$\int_S \left(\frac{e^{ikr}}{r}\frac{\partial v}{\partial n} - v\frac{\partial}{\partial n}\frac{e^{ikr}}{r}\right)dS = \int_0^{4\pi} \left[\varepsilon e^{ik\varepsilon}\left(\frac{\partial v}{\partial r} - ikv\right) + ve^{ik\varepsilon}\right]d\Omega \qquad (60)$$

Since the left-hand side of Eqn. (60) is independent of ε, the limit can be taken as ε approaches zero. Noting that v approaches v_Q (the value of v at point Q) as ε approaches zero, Eqn. (60) reduces to

$$4\pi v_Q = \int_S \left(\frac{e^{ikr}}{r}\frac{\partial v}{\partial n} - v\frac{\partial}{\partial n}\frac{e^{ikr}}{r}\right)dS \qquad (61)$$

where S is any surface which completely encloses the point Q.

Suppose, now, that v represents some monochromatic wave striking a rigid plane barrier with an aperture. For instance, the radiation

of a transducer can be thought of as a plane wave, radiating through some aperture whose shape is the same as the shape of the transducer. Let the plane of the aperture be one portion of S, and let the portion of a large sphere below the aperture, centered at Q, be the remainder of S. As shown by Sommerfeld [9], the integral of Eqn. (61) over this large sphere tends toward zero as the radius of the sphere increases without bound. However, that same result can be argued without resorting to the complex mathematics involved, as shown by Born [8]. His approach was as follows.

A strictly monochromatic wave would have no beginning or ending in time, but a departure can be made from strict monochromaticity as long as the value of v_Q is examined a long time after the beginning of the wave. Because the wave must travel from the aperture with a speed no greater than the velocity of sound in the fluid, there exists some length R, measured from point Q, beyond which the wave has not traveled. Let the radius of the large sphere be R_1, where R_1 is greater than R. Then all along that part of the sphere which makes up the lower portion of S, both v and $\frac{\partial v}{\partial n}$ are zero. Hence, the integral of Eqn. (61) is zero all along this boundary. Let the remainder of S be broken into two parts, with σ denoting the aperture, and σ' the rigid barrier. Then Eqn. (61) becomes

$$4\pi v_Q = \int_{\sigma+\sigma'} \left(\frac{e^{ikr}}{r} \frac{\partial v}{\partial n} - v \frac{\partial}{\partial n} \frac{e^{ikr}}{r}\right) dS \qquad (62)$$

At the barrier, it is reasonable to assume that both v and $\frac{\partial v}{\partial n}$ are zero; thus

$$v = 0 \qquad \text{on } \sigma' \qquad (63)$$
$$\frac{\partial v}{\partial n} = 0$$

and at the aperture

$$v = v' \qquad \text{on } \sigma \qquad (64)$$
$$\frac{\partial v}{\partial n} = \frac{\partial v'}{\partial n}$$

where v' denotes the value that the incident wave would have if the barrier were not present. Because of the boundary conditions expressed by Eqn. (63) the integral over σ' is zero, and the value of v at Q becomes

$$v_Q = \frac{1}{4\pi} \int_\sigma \left(\frac{e^{ikr}}{r} \frac{\partial v'}{\partial n} - v' \frac{\partial}{\partial n} \frac{e^{ikr}}{r}\right) dS \qquad (65)$$

Actually, as shown by Sommerfeld [9], the boundary conditions contained in Eqns. (63) and (64) are mathematically inconsistent, since Eqn. (63) implies that v is zero everywhere. These boundary conditions (Eqns. (63) and (64)) are, however, physically reasonable, even though they are only approximately correct. They are more accurate for high frequencies than low frequencies, and can be used to obtain reasonable estimates of v_Q when the frequency is sufficiently high.

Sommerfeld has modified the auxiliary function used in deriving Kirchoff's diffraction integral in order to eliminate the mathematical inconsistency, but his modification is itself no further justification of the assumed boundary conditions. That is, the inconsistency is removed, but the boundary conditions are still only approximately true,

because the pressure on the downstream side of the baffle is very close to, but not exactly, zero.

To do this, Sommerfeld replaces the auxiliary function u with the Green's function, G, which has the following properties:

$$\begin{aligned} &(\nabla^2 + k^2)G = 0 && \text{in } V \\ &G = 0 && \text{on } \sigma \text{ and } \sigma' \\ &G \to u && \text{as } r \to 0 \end{aligned} \tag{66}$$

Using the first and last conditions, Eqn. (62) becomes

$$4\pi v_Q = \int_{\sigma+\sigma'} \left(G \frac{\partial v}{\partial n} - v \frac{\partial G}{\partial n}\right) dS \tag{67}$$

as before, and the second condition reduces the above equation to

$$4\pi v_Q = -\int_{\sigma+\sigma'} v \frac{\partial G}{\partial n}\, dS \tag{68}$$

Thus, the boundary condition on $\frac{\partial v}{\partial n}$ is not needed, and the mathematical inconsistency is avoided. If v is again assumed to vanish on σ', then v_Q is

$$v_Q = -\frac{1}{4\pi} \int_{\sigma} v \frac{\partial G}{\partial n}\, dS \tag{69}$$

The function G is easy to formulate if the aperture lies in a plane. Shown in Fig. 13 are the aperture, the point Q, a point P in the aperture, and a point R which is the image of Q. The point O is the origin of the ξ, η, and ζ coordinate system which describes the aperture ($\zeta = 0$). The coordinates of Q are (x, y, z),

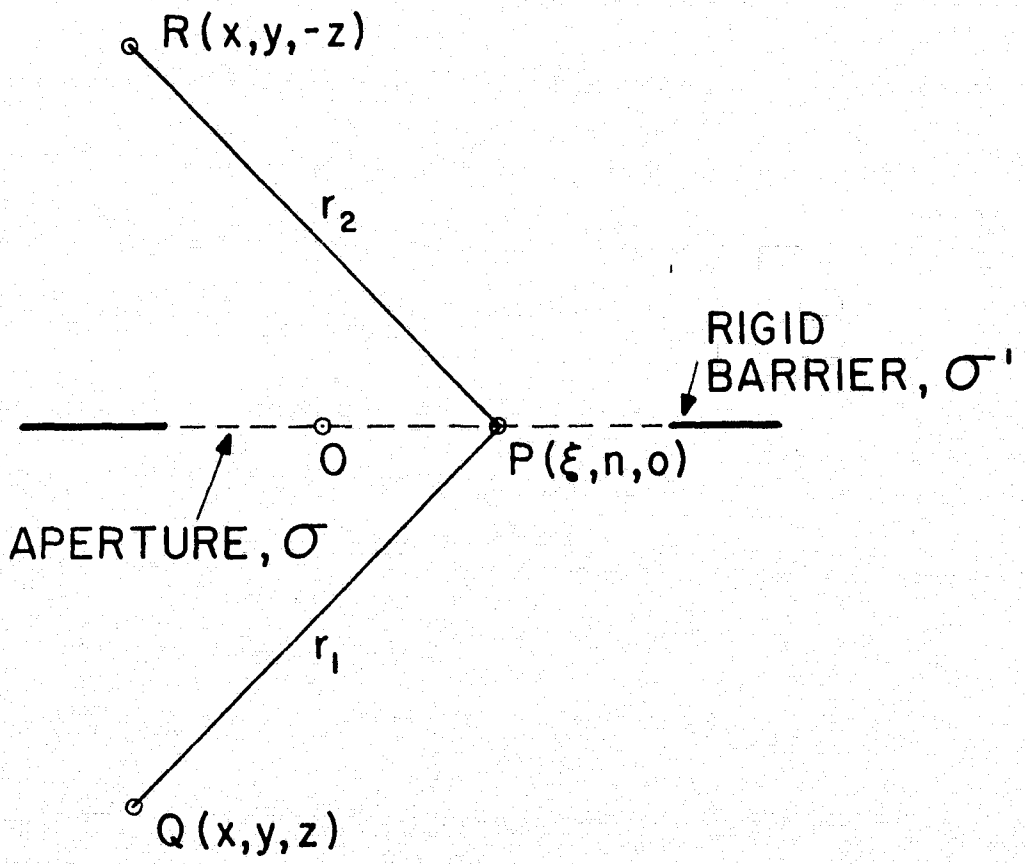

Figure 13

Relationships Defining Green's Function, G

and of R, (x, y, -z). The function G is then defined as

$$G = \frac{e^{ikr_1}}{r_1} - \frac{e^{ikr_2}}{r_2} \tag{70}$$

where

$$r_1^2 = (\xi - x)^2 + (\eta - y)^2 + (\zeta - z)^2 \tag{71}$$

and

$$r_2^2 = (\xi - x)^2 + (\eta - y)^2 + (\zeta + z)^2 \tag{72}$$

For the surface σ, $\frac{\partial}{\partial n} = -\frac{\partial}{\partial \zeta}$, thus

$$\frac{\partial G}{\partial n} = -\frac{\partial G}{\partial r_1}\frac{\partial r_1}{\partial \zeta} - \frac{\partial G}{\partial r_2}\frac{\partial r_2}{\partial \zeta} \tag{73}$$

Substituting, one obtains

$$\frac{\partial G}{\partial n} = \frac{2ze^{ikr}}{r^2}\left(ik - \frac{1}{r}\right) \tag{74}$$

with $r_1 = r_2 = r$ when $\zeta = 0$.

Hence, v_Q is given by

$$v_Q = -\frac{z}{2\pi}\int_\sigma v\,\frac{e^{ikr}}{r^2}\left(ik - \frac{1}{r}\right)dS \tag{75}$$

Since v is any arbitrary function which satisfies Helmholtz's equation, v can be replaced by the pressure of an infinite plane wave. If this pressure is

$$p = Ae^{i(k\zeta - wt)} \tag{76}$$

Eqn. (75) becomes

$$p_Q = -\frac{zA}{2\pi}\int_\sigma \frac{e^{i(kr - wt)}}{r^2}\left(ik - \frac{1}{r}\right)dS \qquad (77)$$

with $\zeta = 0$ on σ. Equation (77) is the pressure at any point downstream of any aperture upon which plane waves are incident, and will be used to describe the diffraction effects of transverse cracks and delaminations upon the sound field produced by the transducer.

Of course, another (or the same) transducer must be used to sense the ultrasonic wave downstream, and the voltage output of this transducer is proportional to the integral of the pressure exerted over its area, σ_R. Using the real part convention, the pressure at any point at a distance z_1 from the sending transducer is given by

$$p_Q = Cz_1\cos wt\int_\sigma \left(\frac{\cos kr}{kr^3} + \frac{\sin kr}{r^2}\right)d\sigma - Cz_1\sin wt\int_\sigma \left(\frac{\cos kr}{r^2} - \frac{\sin kr}{kr^3}\right)d\sigma \qquad (78)$$

The constant of proportionality C is irrelevant since it will be eliminated when a ratio is taken later. Equation (78) is rewritten as,

$$\tilde{p}_Q = A_1\cos wt - A_2\sin wt \qquad (79)$$

in a manner similar to that of Papadakis [10], where A_1 is z_1 times the first integral, and A_2 is z_1 times the second. Thus, the proportional response of the receiving transducer is

$$p_1 = \cos wt \int_{\sigma R} A_1 d\sigma - \sin wt \int_{\sigma R} A_2 d\sigma \tag{80}$$

Equation (80) is rewritten as

$$p_1 = H_1 \cos wt - H_2 \sin wt \tag{81}$$

where H_1 and H_2 are the first and second integrals, respectively. Recalling that the attenuation is obtained from the maximum of p_1, Eqn. (81) is differentiated with respect to time, and set equal to zero, obtaining

$$H_1 \sin wt + H_2 \cos wt = 0 \tag{82}$$

or

$$\tan wt_m = - \frac{H_2}{H_1} \tag{83}$$

where t_m is the time at which p_1 is an extremum. From this

$$\sin wt_m = \frac{\pm H_2}{(H_1^2 + H_2^2)^{1/2}} \tag{84}$$

and

$$\cos wt_m = \frac{\pm H_1}{(H_1^2 + H_2^2)^{1/2}} \tag{85}$$

Substituting Eqns. (84) and (85) back into Eqn. (81), the maximum response of the receiving transducer is found to be

$$p_1 \max = \pm (H_1^2 + H_2^2)^{1/2} \tag{86}$$

The ambiguous sign results from the oscillatory nature of sinusoidals. If the procedure is repeated for some other value of z, say z_2,

then the attenuation due to diffraction is

$$\alpha_D = 20 \log \frac{(p_1 \text{ max})}{(p_2 \text{ max})} \tag{87}$$

where the plus sign has been used in Eqn. (86).

The actual integrations cannot be evaluated in closed form, hence a numerical technique was used. This is discussed next, before proceeding to the theoretical and experimental results.

6. NUMERICAL INTEGRATIONS

The difficulty with finding solutions to problems in terms of integrals, such as was done for the diffraction problem, is that these integrals must eventually be evaluated. This can be done in closed form only for very specific cases, and, in general, some other technique must be used which will yield a good approximation of the desired integral. It is a general rule that the better the approximation, the more complicated is the approximating formula, and vice versa, but a reasonable compromise between accuracy and simplicity exists in a technique known as Gaussian quadratures. A very good reference on the use of quadrature formulae is Kopal [11], and an extension to surface and volume integrals is briefly sketched in Zienkiewicz [12].

Gaussian quadratures can only be used to evaluate integrals with limits of -1 and 1. The approximation for such an integral is

$$\int_{-1}^{1} f(x)dx \simeq \sum_{i=1}^{N} f(a_i)H_i \tag{88}$$

where $f(x)$ is the function to be integrated; $f(a_i)$ is that function evaluated at $x = a_i$; and H_i is the appropriate weighting function for a particular value of a_i. N is the degree of the quadrature formula, and can be any integer larger than two. The H_i's and a_i's are suitably chosen so that Eqn. (88) is exact when $f(x)$ is any polynomial of degree $2N-1$ or less. For example, if N were four, Eqn. (88) would be exact for polynomials of degree seven or less. Values for a_i and H_i are tabulated in references [11] and [12] $N = 2$ to 16.

Most integrals do not have limits of -1 and 1, but a suitable change of variables can transform the integral to one that does. As an example, consider the integral

$$I = \int_{x_1}^{x_2} f(x)dx \tag{89}$$

The linear transformation

$$x = (\frac{x_2 - x_1}{2})\eta + \frac{x_2 + x_1}{2} \tag{90}$$

will suffice, because as x varies from x_1 to x_2, η varies from -1 to 1. Then dx is given by

$$dx = (\frac{x_2 - x_1}{2})d\eta \tag{91}$$

and Eqn. (89) is transformed to

$$I = \int_{-1}^{1} F(\eta)(\frac{x_2 - x_1}{2})d\eta \tag{92}$$

where

$$F(\eta) = f\ [(\frac{x_2 - x_1}{2})\eta + \frac{x_2 + x_1}{2}] \tag{93}$$

In accordance with Eqn. (88), I is then approximated by

$$I \simeq \frac{x_2 - x_1}{2} \sum_{i=1}^{N} H_i\ F(a_i) \tag{94}$$

The change from one-dimensional integration to two-dimensional (surface) integration is only slightly more complicated, as long as the surface of integration is completely contained within a plane.

Consider, first, integrations in polar coordinates. The function to be integrated is $f(r, \theta)$ and the limits on r and θ are r_1 and r_2, and θ_1 and θ_2, respectively. Thus

$$I = \int_{r_1}^{r_2} \int_{\theta_1}^{\theta_2} f(r, \theta) r dr d\theta \tag{95}$$

A change of variables is again necessary, and is performed by

$$\begin{aligned} r &= \left(\frac{r_2 - r_1}{2}\right)\eta + \frac{r_1 + r_2}{2} \\ \theta &= \left(\frac{\theta_2 - \theta_1}{2}\right)\gamma + \frac{\theta_1 - \theta_2}{2} \end{aligned} \tag{96}$$

I is then given by

$$I = \int_{-1}^{1} \int_{-1}^{1} F(\eta, \gamma)\left[\left(\frac{r_2 - r_1}{2}\right)\eta + \frac{r_1 + r_2}{2}\right]\left(\frac{r_2 - r_1}{2}\right)\left(\frac{\theta_2 - \theta_1}{2}\right) d\eta d\gamma \tag{97}$$

Now, let $I_1(\gamma)$, a function of γ, be given by

$$I_1(\gamma) = \int_{-1}^{1} F(\eta, \gamma)\left[\left(\frac{r_2 - r_1}{2}\right)\eta + \left(\frac{r_1 + r_2}{2}\right)\right]\left(\frac{r_2 - r_1}{2}\right) d\eta \tag{98}$$

Then I is given by

$$I = \int_{-1}^{1} I_1(\gamma)\left(\frac{\theta_2 - \theta_1}{2}\right) d\gamma \tag{99}$$

and an application of Eqn. (71) yields

$$I \simeq \left(\frac{\theta_2 - \theta_1}{2}\right) \sum_{i=1}^{N_\gamma} H_i I_1(a_i) \tag{100}$$

where N_γ is used to represent the order of the approximation (number of terms) in γ, or θ. But $I_1(a_i)$ is given by Eqn. (98) when $\gamma = a_i$. Hence

$$I_1(a_i) \simeq \left(\frac{r_2 - r_1}{2}\right) \sum_{j=1}^{N_\eta} F(a_j, a_i)\left[\left(\frac{r_2 - r_1}{2}\right)a_j + \frac{r_1 + r_2}{2}\right]H_j \qquad (101)$$

whence I becomes

$$I \simeq \frac{(\theta_2 - \theta_1)(r_2 - r_1)}{4} \sum_{i=1}^{N_\gamma} \sum_{j=1}^{N_\eta} F(a_j, a_i)H_iH_j\left[\left(\frac{r_2 - r_1}{2}\right)a_j + \frac{r_1 + r_2}{2}\right] \qquad (102)$$

The relationship between the terms in Eqn. (97) and Eqn. (102) is obvious, upon inspection, and once Eqn. (97) is written, Eqn. (102) can be deduced immediately, without need of the intervening steps.

As a final example, consider the integration of the function $f(x, y)$ over the region defined by

$$g_1(x) \leq y \leq g_2(x) \quad \text{when} \quad x_1 \leq x \leq x_2 \qquad (103)$$

The desired integral is

$$I = \int_{x_1}^{x_2} \int_{g_1(x)}^{g_2(x)} f(x, y)dxdy \qquad (104)$$

The variables x and y are transformed by

$$x = \left(\frac{x_2 - x_1}{2}\right)\eta + \left(\frac{x_2 + x_1}{2}\right) \qquad (105)$$

and

$$y = \left[\frac{G_2(\eta) - G_1(\eta)}{2}\right]\gamma + \frac{G_2(\eta) + G_1(\eta)}{2} \qquad (106)$$

where

$$G_i(\eta) = g_i[(\frac{x_2 - x_1}{2})\eta + \frac{x_2 + x_1}{2}] \tag{107}$$

From Kreyszig [13]

$$dxdy = [\frac{\partial x}{\partial \eta}\frac{\partial y}{\partial \gamma} - \frac{\partial x}{\partial \gamma}\frac{\partial y}{\partial \eta}]d\eta d\gamma \tag{108}$$

or

$$dxdy = (\frac{x_2 - x_1}{2})[\frac{G_2(\eta) - G_1(\eta)}{2}]d\eta d\gamma \tag{109}$$

and Eqn. (104) becomes

$$I = \int_{-1}^{1}\int_{-1}^{1} F(\eta, \gamma)\frac{(x_2 - x_1)}{4}[G_2(\eta) - G_1(\eta)]d\eta d\gamma \tag{110}$$

whereupon I is approximated by

$$I \simeq \frac{x_2 - x_1}{4}\sum_{i=1}^{N_\gamma}\sum_{j=1}^{N_\eta} F(a_j, a_i)[G_2(a_j) - G_1(a_j)]H_iH_j \tag{111}$$

Equation (111), then, is an approximation appropriate for any surface integral in the $x - y$ plane. The actual formulas used in finding the diffraction losses are given in the appendix, as well as the computer programs used to evaluate them. The results of the numerical computations are discussed next.

7. NUMERICAL RESULTS

To simplify the calculations required to find the diffraction losses due to damage development in composites, certain assumptions must be made. These assumptions are not justified by any physical arguments, but, in as much as this text is meant to be of an exploratory rather than of a definitive nature, they are acceptable as a first approach to solution. The specimen is assumed to be infinitesimally thin, and serves only to cover the transducer in damaged areas (locations of cracks or delaminations). Replacing the fused silica delay block with an inviscid fluid has already been discussed, but, inherent in this substitution is the assumption of no attenuation in the quartz, which is only approximately correct. Also implied in Eqn. (77) is that the wave is monochromatic, which is, of course, not true in pulse-echo work. The next approximation applies only to the diffraction effects calculated for transverse cracks, and is obtained as follows.

For high frequency waves, k is much larger than $\frac{1}{r}$, except for small r, and Eqn. (77) can be simplified to

$$p_Q = - \frac{izkA}{2\pi} \int_\sigma \frac{e^{i(kr - wt)}}{r^2} dS \qquad (112)$$

Another simplification is afforded if z is assumed large enough so that the ratio $\frac{z}{r}$ is approximately one for the values of r which occur in the integrand. Then Eqn. (112) becomes

$$p_Q = -\frac{ikA}{2\pi}\int_{\sigma}\frac{e^{i(kr - wt)}}{r}\,dS \qquad (113)$$

which is essentially the formula used by Papadakis [10].

Since this report is concerned mainly with pulse-echo measurements, the sending transducer is assumed to be the same as the receiving transducer, though it is displaced in the z-direction by increments of $2nL$ to account for the distance traveled by each echo. But more importantly, the receiving transducer is covered by exactly the same cracks, in exactly the same location, as the sending transducer.

Let the area of the transducer be denoted by A_T, and that of the cracks by A_C. To differentiate between the sending and receiving transducer, a superscript of S or R will be used with the appropriate area. Then the response of the receiving transducer will be proportional to (real part convention)

$$\tilde{p} = \int_{(A_T^R - A_C^R)}\int_{(A_T^S - A_C^S)}\frac{e^{i(kr - wt)}}{r}\,d\sigma^S d\sigma^R \qquad (114)$$

which can be expanded into the form

$$\tilde{p} = \left\{\left[\int_{A_T^R}\int_{A_T^S} - \int_{A_C^R}\int_{A_T^S} - \int_{A_T^R}\int_{A_C^S} + \int_{A_C^R}\int_{A_C^S}\right]\frac{e^{i(kr - wt)}}{r}\,d\sigma^R d\sigma^S\right\} \qquad (115)$$

It is a fairly simple matter to show that the second and third integrals are exactly equal. The last integral is assumed to be small

enough to neglect, and Eqn. (115) is rewritten

$$\tilde{p} = \int_{A_T^R} \int_{A_T^S} \frac{e^{i(kr - wt)}}{r} d\sigma^R d\sigma^S - 2 \int_{A_T^R} \int_{A_C^S} \frac{e^{i(kr - wt)}}{r} d\sigma^R d\sigma^S \tag{116}$$

Equation (116) was used, instead of the more exact formulation of Eqn. (115), to greatly reduce the amount of computing time required. The first integral of Eqn. (116) is of special interest because it is used to find the diffraction losses from the transducer alone.

7.1 Accuracy of the Integration Techniques

The pressure at any point along the axis of the sending transducer can be obtained in closed form by integrating Eqn. (77). If z is the distance from the transducer to the point on the axis, and if D is given by

$$D = (R^2 + z^2)^{1/2} \tag{117}$$

where R is the radius of the transducer, then the pressure at any point Q $(0, 0, z)$ is

$$p_Q = \left[1 + \frac{z^2}{D^2} - 2 \frac{z}{D} \cos k (D - z)\right]^{1/2} \tag{118}$$

Because the integration of Eqn. (77) to obtain Eqn. (118) is the same type of integration used later to calculate the attenuation due to diffraction, this was considered to be an ideal means of checking the accuracy of the Gaussian quadrative formulae. This check was performed in both rectangular and polar coordinates, since they were

to be used in the later calculations. Three values of k (16π, 20π and 24π) were used because they correspond to the range of frequencies used in the laboratory (4.8, 6, and 7.2 MHz, respectively). Table IV presents the results of the numerical integrations in both coordinate systems, as well as the exact answers. The results for all three values of k were very similar, and only the results for $k = 20\pi$ are presented. Note that the polar coordinate formula is very accurate for all but the smallest values of z. The rectangular formula is less so, but is sufficiently accurate for the values of z required (z greater than 1.0 cm).

7.2 Diffraction by Transverse Cracks

Because it is necessary to evaluate the diffraction integral numerically, rather than in closed form, it is possible to find the diffraction losses for only a finite number of cases out of the infinite combinations of crack location, length, shape, width, and operating frequency which can exist. It was decided, then, to choose a maximum of four crack spacings, three crack widths, and three frequencies for a total of thirty-six possible combinations, while the cracks were assumed to be rectangular in shape, and to extend completely across the width of the specimen. The cracks were also assumed to be evenly spaced across the width of the transducer so that symmetry could be used to reduce the amount of camputation time required. The crack spacings used were 0.075 cm, 0.098 cm, 0.141 cm, and 0.254 cm. The radius of the transducer used was .635 cm, and for this size transducer, the above spacings correspond to 16, 12, 8, and 4 cracks, respectively,

TABLE IV

COMPARISON OF THE EXACT FORMULATION AND GAUSSIAN APPROXIMATION OF THE PRESSURE ALONG THE AXIS OF THE TRANSDUCER ($k = 20\pi$)

z (cm.)	Exact Pressure	Gaussian Approximations	
		Rectangular	Polar
0	1.000	0.000	0.000
0.001	1.001	0.116	0.770
0.01	1.000	1.152	0.985
0.02	0.982	2.248	0.982
0.05	0.948	4.781	0.948
0.10	1.142	5.553	1.142
0.20	1.192	0.718	1.192
0.50	0.554	0.540	0.554
0.80	1.123	1.124	1.123
1.0	0.870	0.869	0.870
1.5	1.514	1.514	1.514
2.0	0.109	0.109	0.109
5.0	1.898	1.898	1.898
7.5	1.491	1.491	1.491
10.0	1.182	1.182	1.182
25.0	0.501	0.501	0.501
50.0	0.253	0.253	0.253
75.0	0.169	0.169	0.169
100.0	0.127	0.127	0.127

across the total width of the transducer. As was mentioned earlier, the frequencies used were 4.8, 6, and 7.2 MHz, and the cracks were assumed to be 0.008, 0.016, or 0.024 cm. wide. Of the possible thirty-six cases, twenty-three were actually used; specifically, they were:

1) 4.8 MHz ($k = 16\pi$)
   a) 8 cracks, all three widths
   b) 16 cracks, all three widths
2) 6.0 MHz ($k = 20\pi$)
   a) 4 cracks, 0.016 and 0.024 cm wide
   b) 8 cracks, all three widths
   c) 12 cracks, all three widths
   d) 16 cracks, all three widths
3) 7.2 MHz ($k = 24\pi$)
   a) 8 cracks, all three widths
   b) 16 cracks, all three widths

The diffraction curves for the above cases are presented in Figs. 14 through 21. The horizontal scale is the distance z traveled by the wave, divided by the length of the delay block, 2.55 cm. The first echo, then, is at $z/L = 2$, and the second at $z/L = 4$. Included in each figure is the diffraction loss curve for the transducer alone. The following procedure is then used to find the attenuation change that would occur for the given damage state.

The original diffraction loss is found by taking the difference in the heights of the transducer loss curve between $z/L = 2$ and

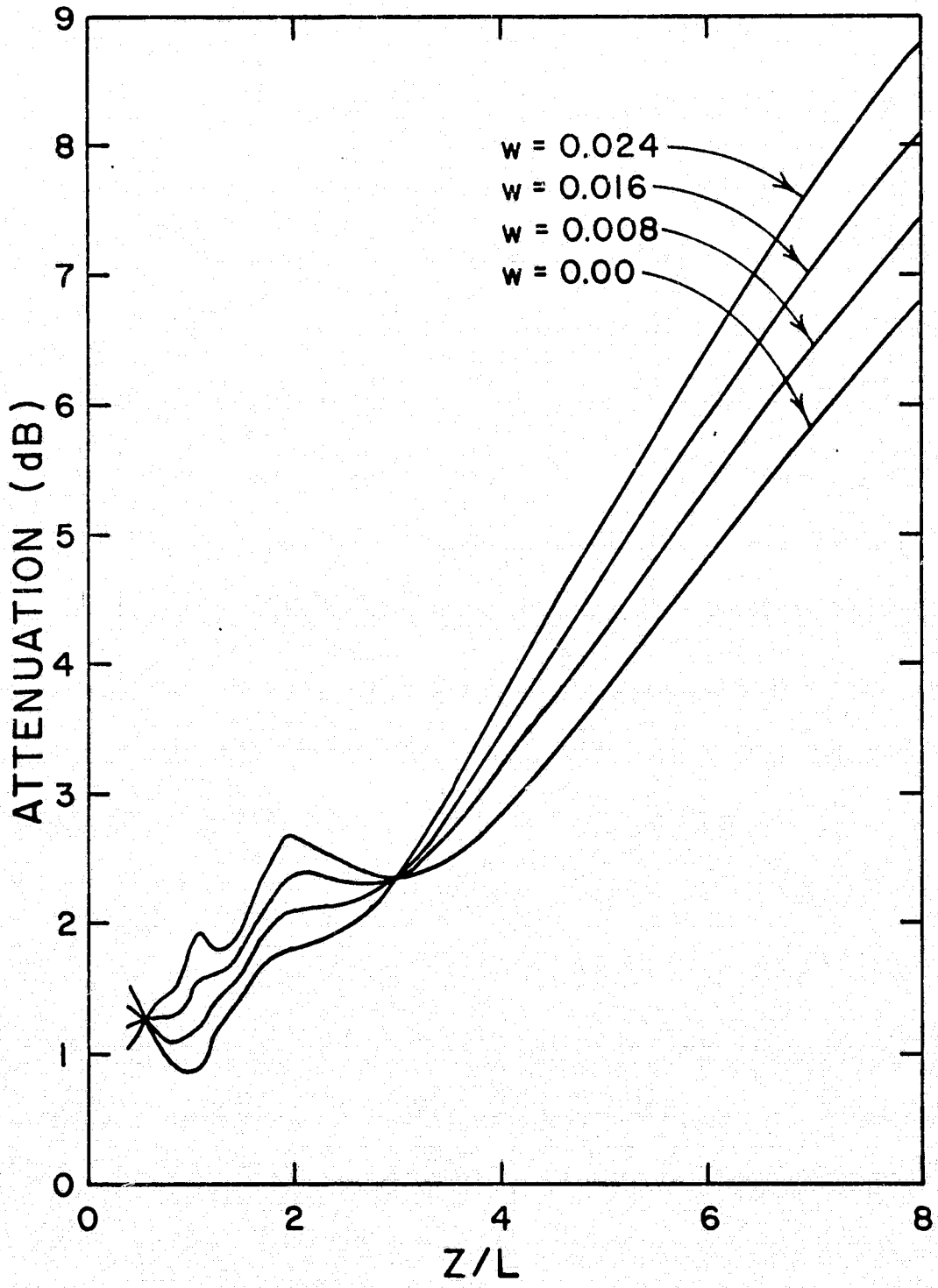

Figure 14. Attenuation vs. z/L for 4.8 MHz, 8 Cracks

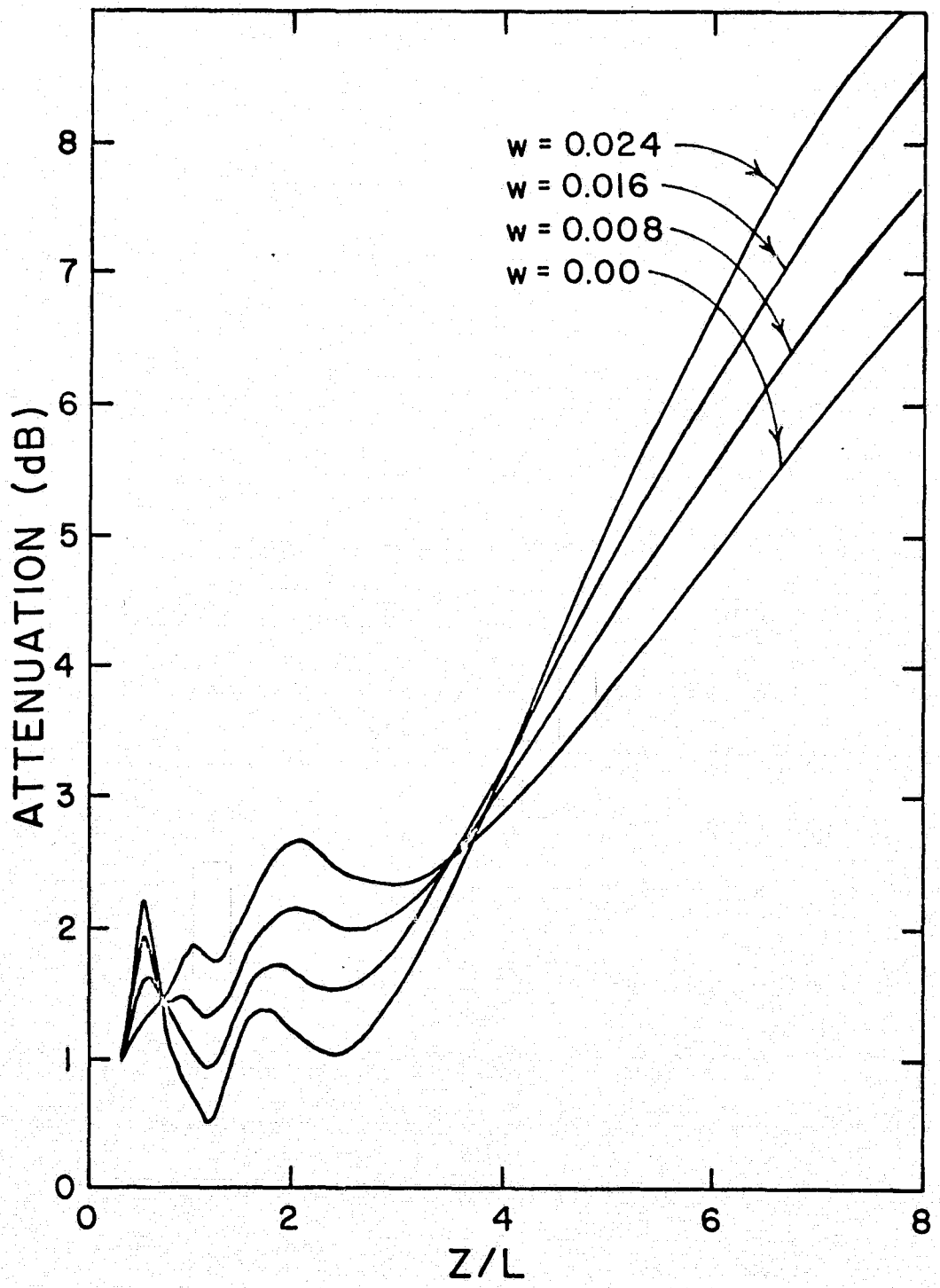

Figure 15. Attenuation vs. z/L for 4.8 MHz, 16 Cracks

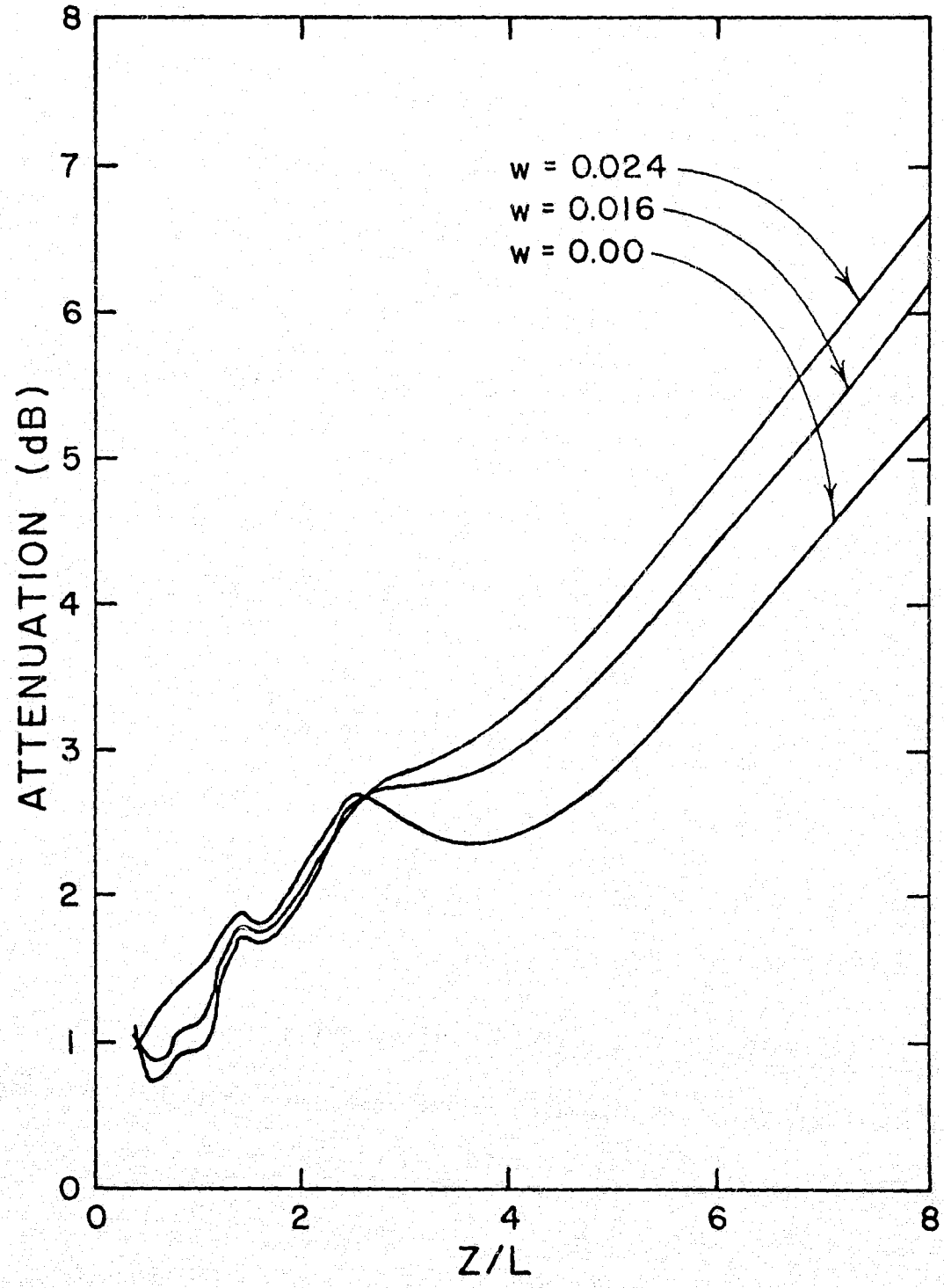

Figure 16. Attenuation vs. z/L for 6.0 MHz, 4 Cracks

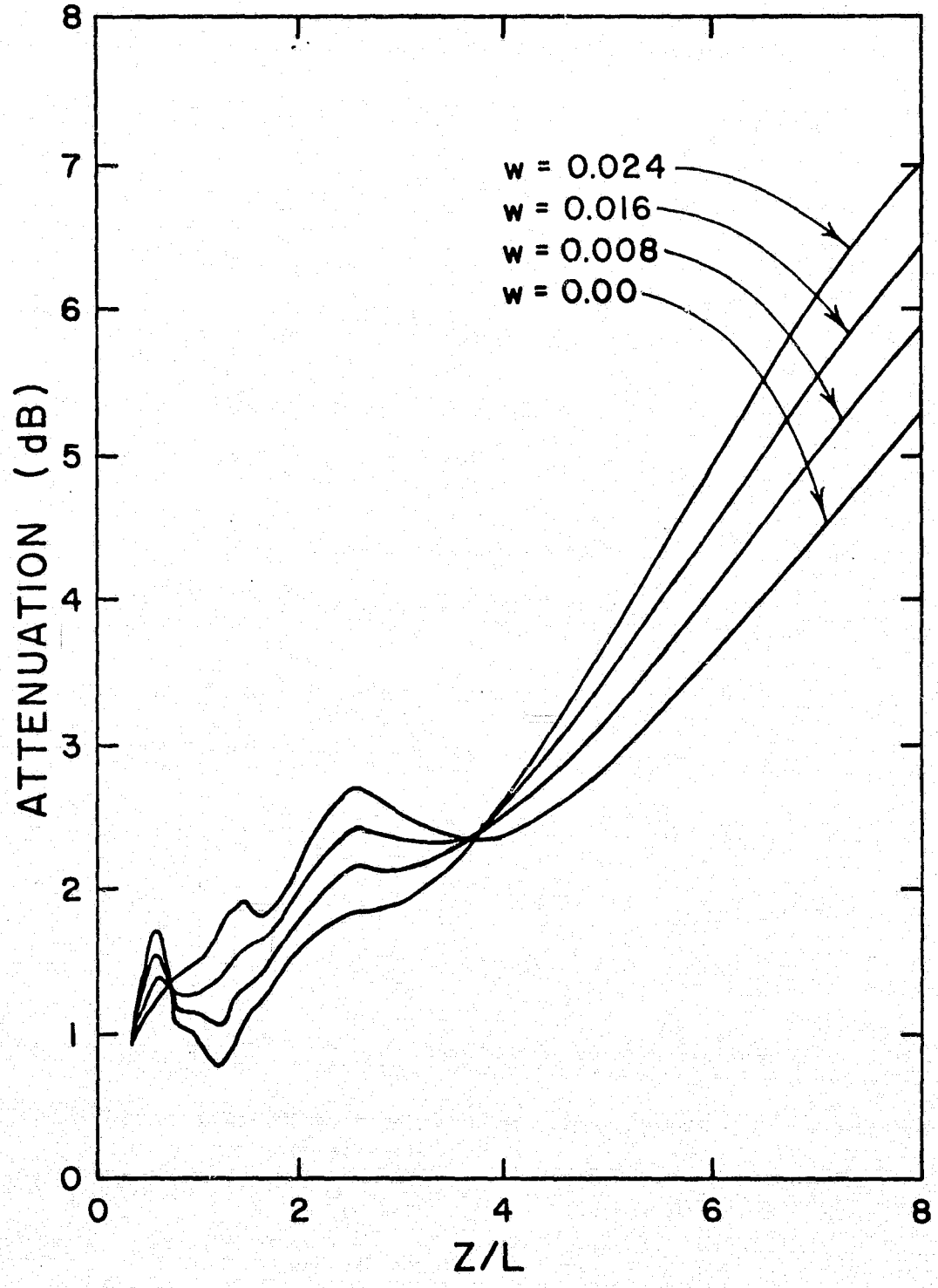

Figure 17. Attenuation vs. z/L for 6.0 MHz, 8 Cracks

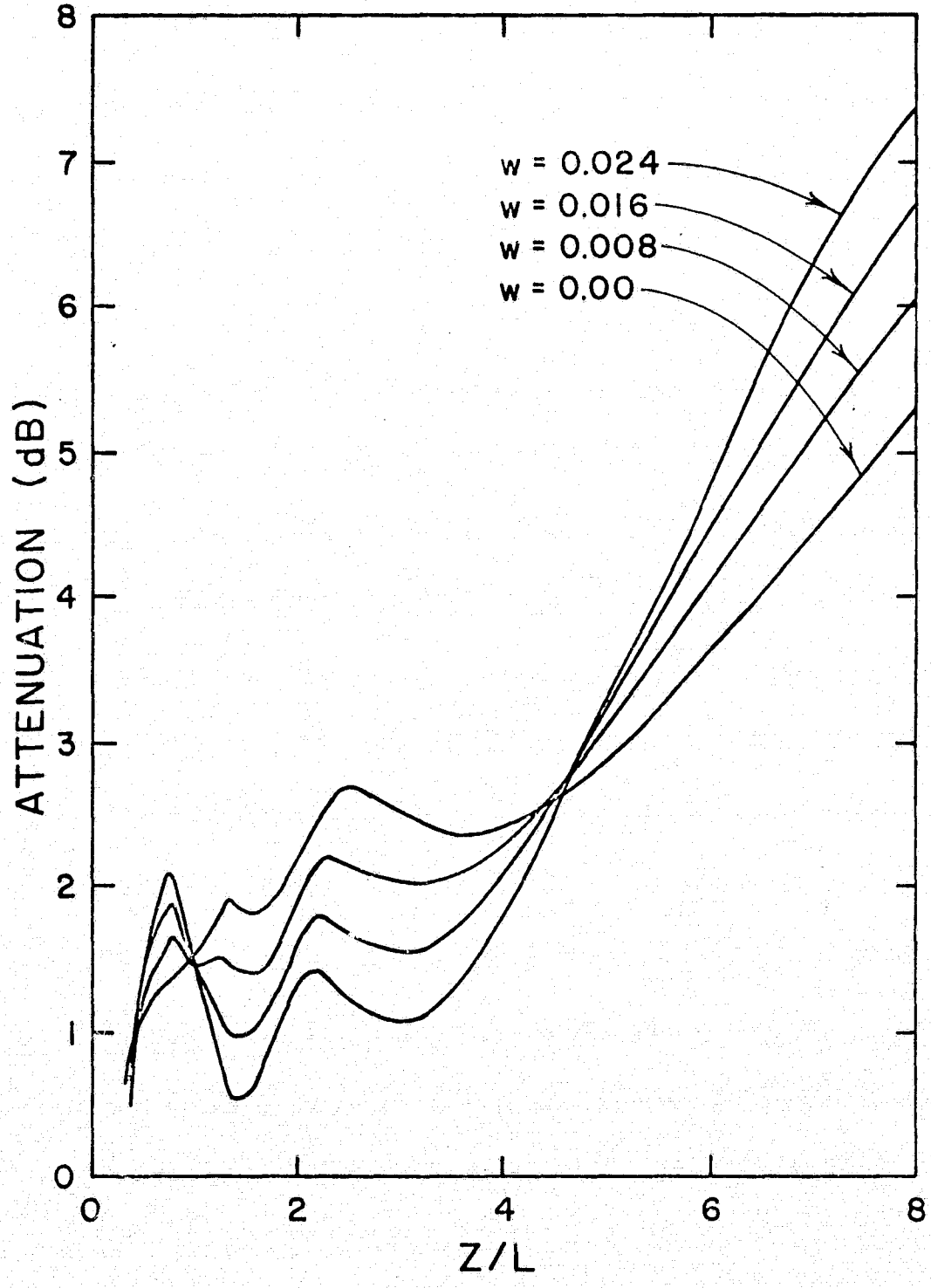

Figure 18. Attenuation vs. z/L for 6.0 MHz, 12 Cracks

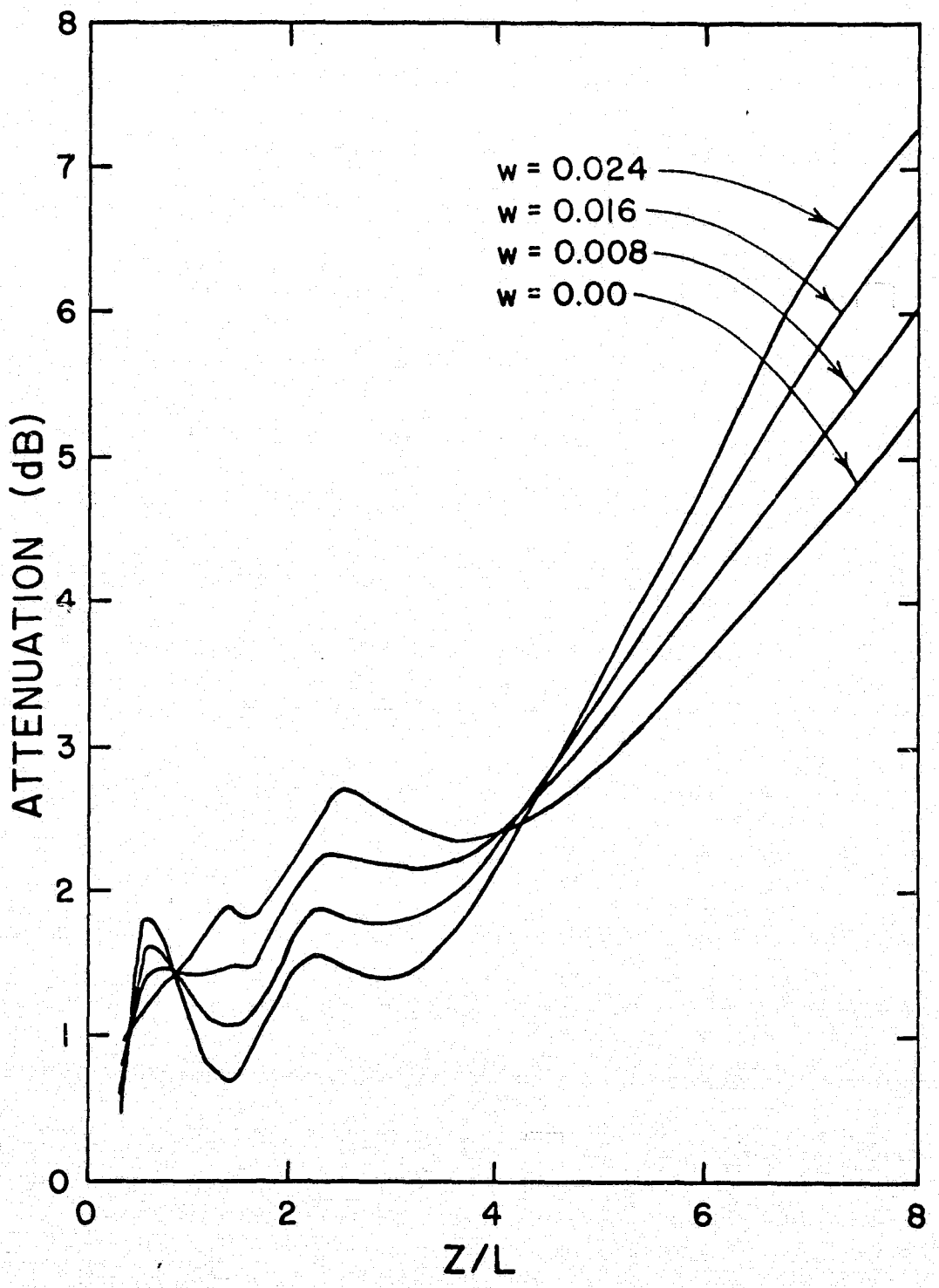

Figure 19. Attenuation vs. z/L for 6.0 MHz, 16 Cracks

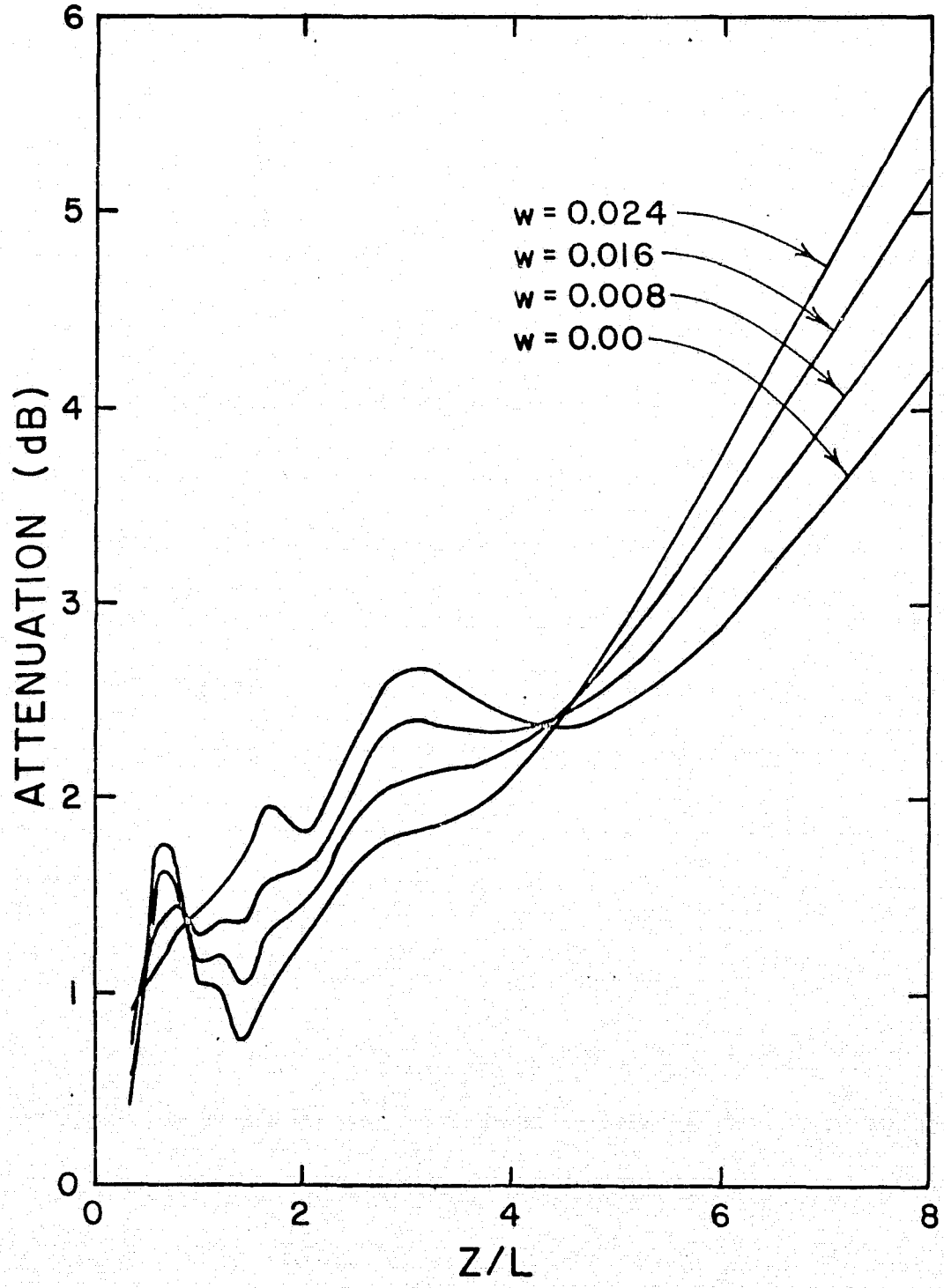

Figure 20. Attenuation vs. z/L for 7.2 MHz, 8 Cracks

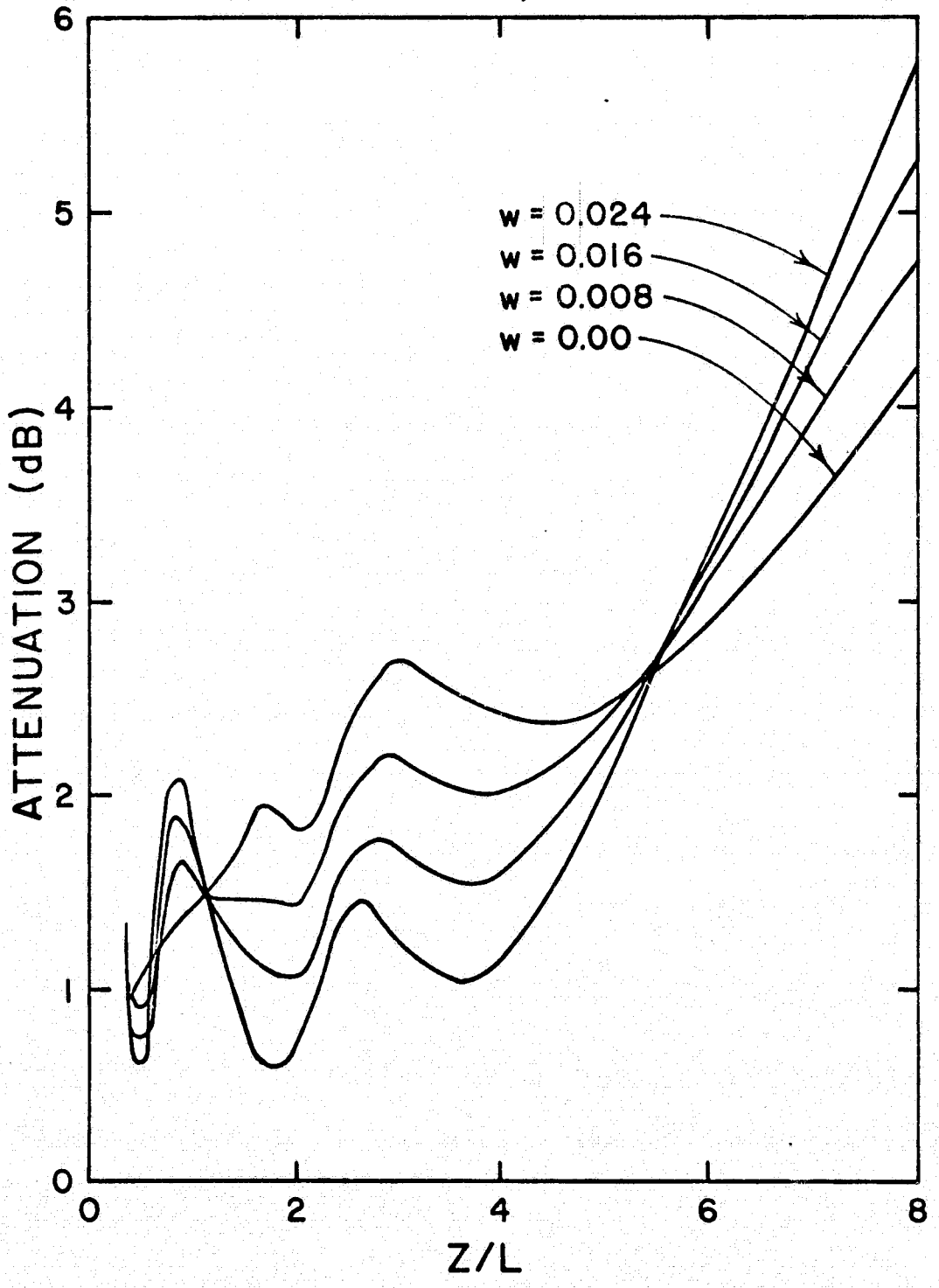

Figure 21. Attenuation vs. z/L for 7.2 MHz, 16 Cracks

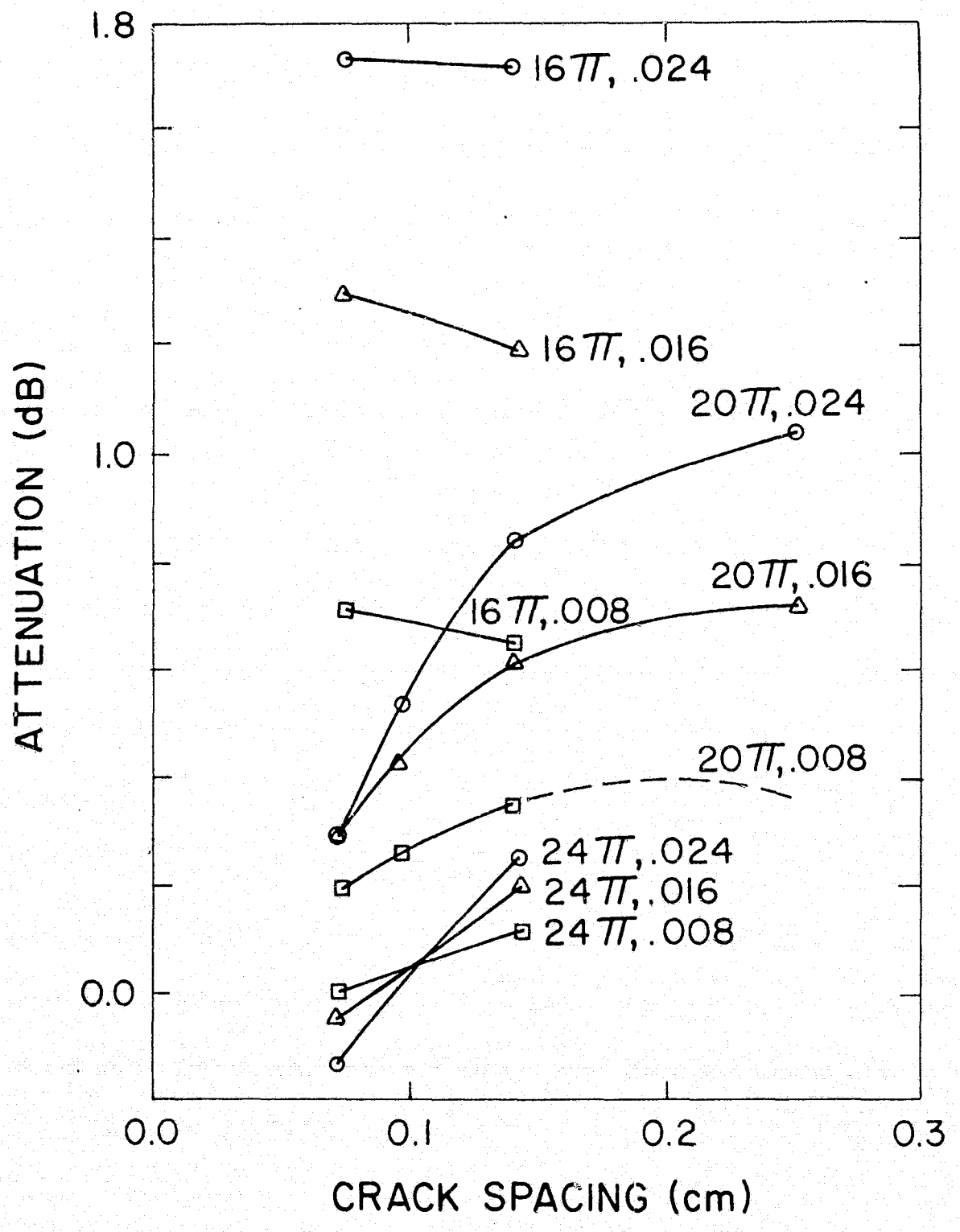

Fig. 22 Attenuation vs. Crack Spacing

$z/L = 4$. For example, in Fig. 14, where $k = 16\pi$, this difference is 0.21 dB. After 8 cracks, 0.016 cm wide, have completely formed, the loss, again found by taking the difference on the appropriate curve, is 0.86 dB. Thus, there is a net change of 0.65 dB. The results for all twenty-three cases are presented in Table V.

Several facts are of note. Firstly, by examining the column for the transducer losses, one can see that an increase in operating frequency is not always accompanied by a decrease in the initial attenuation, as is commonly believed. Secondly, an increase in the number of cracks present does not necessarily mean an increase in the diffraction losses, as is evidenced by the listings under 6.0 and 7.2 MHz, although the above is true at 4.8 MHz. And thirdly, the net change can be negative; i.e., the apparent attenuation of the specimen may decrease as more damage is introduced.

Even though insufficient cases have been examined to properly generalize the above results, Fig. 22 is presented as a graph of the expected attenuation change versus crack spacing with frequency and crack width as parameters. No strict conclusions should be drawn from this graph until more data has been obtained. It is shown here merely as an aid to visualization of the results in Table V.

From these results, it is readily apparent that frequency plays a major role in the amount of change which can be expected. By simply varying the frequency from 4.8 to 7.2 MHz, the diffraction loss for one case would change from 1.74 dB to -0.14 dB, a net difference of almost 2 dB (Recall, though, that the bond loss term can also vary quite a bit with frequency, overwhelming more minor

TABLE V

DIFFRACTION LOSSES OF VARIOUS CRACK SPACINGS AND WIDTHS

Freq. (MHz)	No. of Cracks	Crack Width (cm)	Loss from Transducer (dB)	Loss from Cracks (dB)	Net Loss (dB)
4.8	8	.008	0.21	0.86	0.65
		.016		1.39	1.18
		.024		1.93	1.72
	16	.008		0.93	0.72
		.016		1.51	1.30
		.024		1.95	1.74
6.0	4	.016	0.20	0.91	0.71
		.024		1.25	1.05
	8	.008		0.54	0.34
		.016		0.81	0.61
		.024		1.04	0.84
	12	.008		0.46	0.26
		.016		0.63	0.43
		.024		0.73	0.53
	16	.008		0.40	0.20
		.016		0.49	0.29
		.024		0.49	0.29
7.2	8	.008	0.59	0.71	0.12
		.016		0.79	0.20
		.024		0.83	0.24
	16	.008		0.59	0.0
		.016		0.54	-0.05
		.024		0.45	-0.14

changes in the diffraction loss). Obviously, the frequency at which these tests are conducted in the future should be strictly controlled and accurately measured.

7.3 Diffraction by Delaminations

To calculate the diffraction effects of delaminations, it was assumed that a transducer with a diameter of 0.5 in. was centered on a specimen 1 in wide. The boundaries of the delaminations were assumed to be straight lines, parallel to the edges of the specimen, which have progressed to equal depths on either side of the specimen. Of course, until the delaminations are a quarter of an inch deep, they will have no effect on the transducer, and the apparent attenuation due to diffraction is the same as for the transducer itself. If the delaminations are a half of an inch deep, they completely cover the specimen, and no sound will pass through. The diffraction loss curves for various depths of delaminations are shown in Fig. 23 for $k = 20\pi$. The expected losses for the 1 inch long delay block were calculated as detailed above, and are presented in Fig. 24. Note that the expected losses are fairly insignificant until the delaminations penetrate to about 0.29 in., but that they rise fairly quickly after that point, reaching 2.8 dB when the depth is 0.4 in. The predicted loss is around one-half of a decibel when the depth of penetration is only 0.31 in., again attesting to the speed with which the attenuation rises once the delaminations penetrate beyond the critical depth of 0.29 in.

The fact that delaminations have not generally been found to

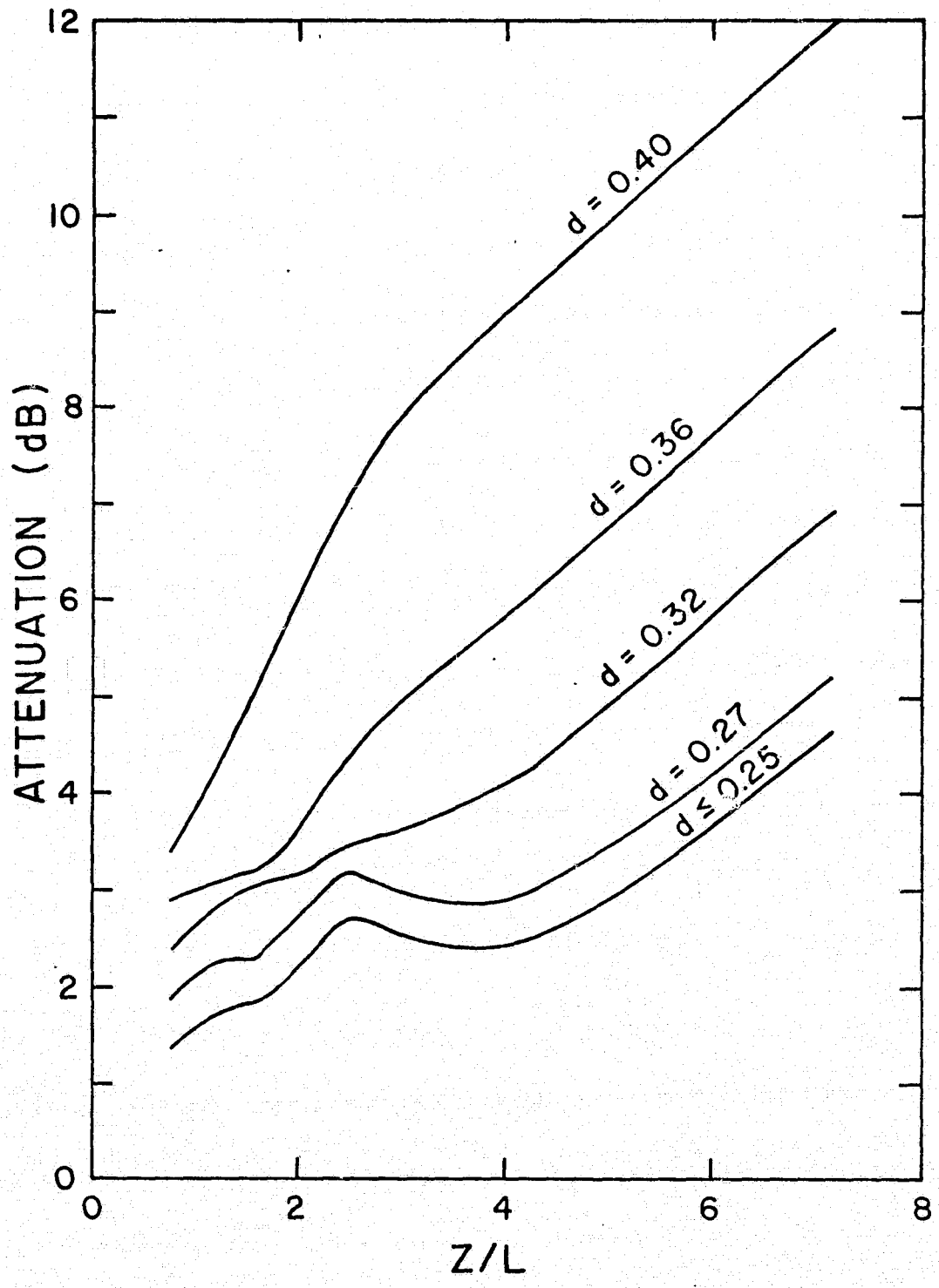

Figure 23. Attenuation vs. z/L for various Depth Delaminations, 6.0 MHz

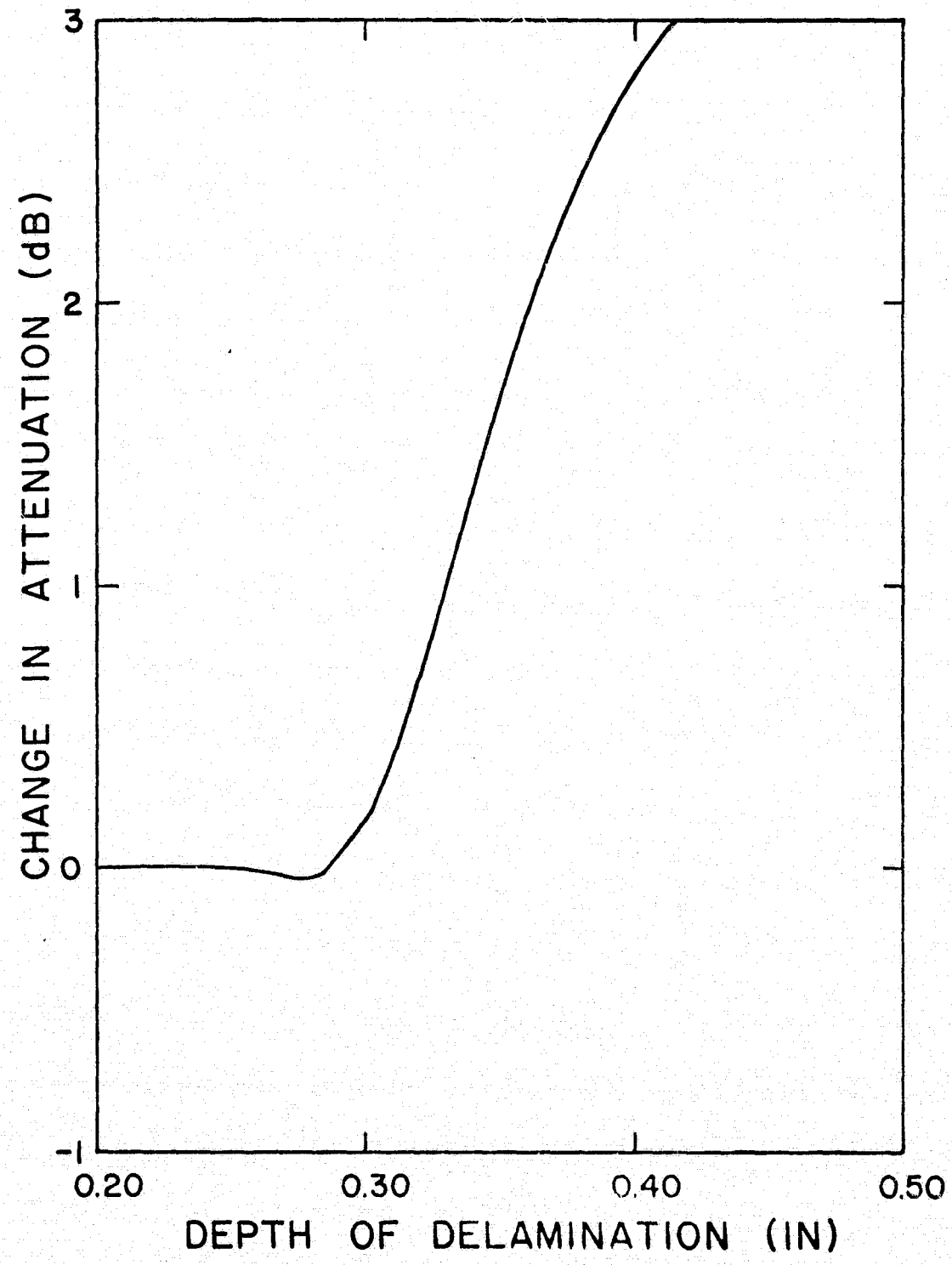

Figure 24. Change in Attenuation vs. Delamination Depth

penetrate more than a quarter of an inch into the width is not a serious problem, since the transducer is usually not well centered on the specimen. A displacement of a tenth of an inch from the center is not unusual (in fact, it is quite likely) and would result in extensive coverage of one side of the transducer.

8. CONCLUSIONS AND SUMMARY

From this study, it is apparent that the existence of transverse cracks or delaminations can indeed account for the changes in attenuation which occur as specimens are loaded in quasi-static tension, and thus, these changes could serve as an indicator of damage formation and growth in the specimens in regions not readily accessible to visual observation. Moreover, the predicted changes are well within the range of values found experimentally, and also show both increasing and decreasing trends evidenced by experiments. Both the amount and the direction of the change are closely related to the frequency used in the test. In the future, the frequency should be closely controlled.

It is the as yet unproven contention of the author that the very sudden rises in attenuation are caused by damage formation, such as a transverse crack appearing, while the more slow and gradual changes are due to such phenomena as the already existing cracks opening wider under load; and that both the rapidity and the amount of such changes can give some details as to damage formation and growth.

Because of the general nature of this work, little emphasis was placed on obtaining exact correlations for specific specimens. Studies of this type are certainly in order, as are also investigations of errors, such as improperly functioning transducers, which can mask or distort the experimental data.

With the improvements which are sure to arise from additional

investigations, the method described here-in appears to be of some aid to investigators studying the formation and growth of damage in thin composite laminates.

9. REFERENCES

[1] Jones, R. M., Mechanics of Composite Materials, McGraw-Hill, New York, 1975

[2] Pagano, N. J. and Pipes, R. B., "Some Observations on the Interlaminar Strength of Composite Laminates", International Journal of Mechanical Science, Vol. 15, 1973, pp. 679-688

[3] Reifsnider, K. L., "Some Fundemental Aspects of the Fatigue and Fracture Response of Composite Materials", (to be published)

[4] Pagano, N. J., "Failure Mechanisms and Criteria in Composite Materials", Mechanics of Composites Review, October, 1976, pp. 183-198

[5] Truell, R., Elbaum, C., and Chick, B. B., Ultrasonic Methods in Solid State Physics, Academic Press, New York, 1969

[6] Papadakis, E. P., "Ultrasonic Attenuation in Thin Specimens Driven Through Buffer Rods", Journal of the Acoustical Society of America, Vol. 44, No. 3, September, 1963, pp. 724-734

[7] Hayford, D. T., Henneke, E. G., Stinchcomb, W. W., "A Technique For Determining an Absolute Value of Ultrasonic Attenuation in Thin, Composite Laminates", Journal of Composite Materials (to be published)

[8] Born, M., and Wolf, E., Principles of Optics, Pergammon Press, Oxford, 1965

[9] Sommerfeld, A. E., Optics, Academic Press, New York, 1967

[10] Papadakis, E. P., "Ultrasonic Diffraction from Single Apertures with Application to Pulse Measurements and Crystal Physics", Physical Acoustics, Vol. XI, Mason, W. P. and Thurston, R. N., eds., Academic Press, New York, 1975

[11] Kopal, Z., Numerical Analysis, Chapman and Hall, 1961

[12] Zienkiewicz, O. C., The Finite Element Method in Structural and Continuum Mechanics, McGraw-Hill, London, 1967

[13] Kreyszig, E., Advanced Engineering Mathematics, John Wiley and Sons, New York, 1968

A. APPENDIX

The integral equations described earlier, along with their approximation formulae are listed below.

A.1 The Pressure Along the Axis of the Transducer

The maximum pressure at some point lying on the axis of the sending transducer is

$$p_Q = (H_1^2 + H_2^2)^{1/2} \tag{119}$$

In radial coordinates, H_1 and H_2 are given by

$$H_1 = zk \int_0^R \left(\frac{\cos kr}{kr^3} + \frac{\sin kr}{r^2}\right)\rho d\rho \tag{120}$$

and

$$H_2 = zk \int_0^R \left(\frac{\cos kr}{r^2} - \frac{\sin kr}{kr^3}\right)\rho d\rho \tag{121}$$

The approximations for the above are

$$H_1 \simeq \frac{zkR^2}{4} \sum_{i=1}^{16} h_i (1 + a_i) \left[\frac{\cos kr}{kr^3} + \frac{\sin kr}{r^2}\right] \tag{122}$$

and

$$H_2 \simeq \frac{zkR^2}{4} \sum_{i=1}^{16} h_i (1 + a_i) \left[\frac{\cos kr}{r^2} - \frac{\sin kr}{kr^3}\right] \tag{123}$$

where a_i and h_i are the Gaussian quadrature constants. The numerical value of r is

$$r = \left[\frac{R^2}{4}\left(1 + a_i^2\right) + z^2\right]^{1/2} \tag{124}$$

In rectangular coordinates, H_1 and H_2 are approximated by

$$H_1 \simeq \frac{zkR^2}{2\pi} \sum_{i=1}^{16} \sum_{j=1}^{16} h_i\, h_j \left(1 - a_i^2\right)^{1/2} \left[\frac{\cos kr}{kr^3} + \frac{\sin kr}{r^2}\right] \tag{125}$$

and

$$H_2 \simeq \frac{zkR^2}{2\pi} \sum_{i=1}^{16} \sum_{j=1}^{16} h_i\, h_j \left(1 - a_i^2\right)^{1/2} \left[\frac{\cos kr}{r^2} - \frac{\sin kr}{kr^3}\right] \tag{126}$$

where

$$r = \left[\frac{R^2}{4} a_i^2 + \frac{R^2}{4}\left(1 - a_i^2\right)a_j^2 + z^2\right]^{1/2} \tag{127}$$

A.2 The Pressure on the Receiving Transducer with No Damage

Using the approximation detailed in Section 7, the average pressure on the receiving transducer is

$$\tilde{p} = \left(H_1^2 + H_2^2\right)^{1/2} \tag{128}$$

where

$$H_1 = 2\pi \int_0^{2\pi} \int_0^{R} \int_0^{R} \frac{\cos kr}{r}\, \rho\, d\rho\, \eta\, d\eta\, d\theta \tag{129}$$

and

$$H_2 = 2\pi \int_0^{2\pi} \int_0^{R} \int_0^{R} \frac{\sin kr}{r}\, \rho\, d\rho\, \eta\, d\eta\, d\theta \tag{130}$$

where

$$r = [(\eta\cos\theta - \rho)^2 + \eta^2\sin^2\theta + z^2]^{1/2} \tag{131}$$

The approximation formulae are

$$H_1 \simeq \frac{R^4\pi^2}{16} \sum_{i=1}^{16} \sum_{j=1}^{2} \sum_{m=1}^{16} \sum_{n=1}^{16} (1 + a_i)(1 + a_m)\, h_i\, h_m\, h_n \frac{\cos kr}{r} \tag{132}$$

and

$$H_2 \simeq \frac{R^4\pi^2}{16} \sum_{i=1}^{16} \sum_{j=1}^{2} \sum_{m=1}^{16} \sum_{n=1}^{16} (1 + a_i)(1 + a_m)\, h_i\, h_m\, h_n \frac{\sin kr}{r} \tag{133}$$

where

$$r = \{\frac{R^2}{4}[(1 + a_m)\cos\theta_{jn} - (1 + a_i)]^2 + \frac{R^2}{4}(1 + a_m)^2 \sin^2\theta_{jn} + z^2\} \tag{134}$$

and

$$\theta_{jn} = \frac{\pi}{4}[(2j - 1) + a_n] \tag{135}$$

A.3 Response of the Receiving Transducer in the Presence of Transverse Cracks

As discussed in Section 7, H_1 and H_2 were modified by subtracting the integrals denoted by H_1' and H_2' below. Otherwise Eqn. (128) still applies in finding the average pressure on the receiving transducer. H_1' and H_2' are

$$H_1' = 2 \int_{A_C} \int_0^{2\pi} \int_0^R \frac{\cos kr}{r} \rho d\rho d\theta d\sigma^C \tag{135}$$

$$H_2' = 2 \int_{A_C} \int_0^{2\pi} \int_0^R \frac{\sin kr}{r} \rho d\rho d\theta d\sigma^C \tag{136}$$

The integration over the area of the cracks was done with a 16-point quadrature formula in the y direction and a 4-point formula in the x direction. Let x_i denote the centerline of a crack, and w the width of a crack. The height of the crack is y_i, and is given by

$$y_i = (R^2 - x_i^2)^{1/2} \tag{137}$$

The approximations for H_1' and H_2' are

$$H_1' \simeq \frac{\pi R^2 w}{8} \sum_{i=1}^{NC} \sum_{j=1}^{16} \sum_{\ell=1}^{4} \sum_{m=1}^{16} \sum_{n=1}^{16} \sum_{s=1}^{2} h_j h_\ell h_m h_n (1 + a_m) y_i \frac{\cos kr}{r} \tag{138}$$

$$H_2' = \frac{\pi R^2 w}{8} \sum_{i=1}^{NC} \sum_{j=1}^{16} \sum_{\ell=1}^{4} \sum_{m=1}^{16} \sum_{n=1}^{16} \sum_{s=1}^{2} h_j h_\ell h_m h_n (1 + a_m) y_i \frac{\sin kr}{r} \tag{139}$$

where NC is the number of cracks. To formulate r, let

$$R_1 = \frac{R}{2} (1 + a_m) \cos\theta_{sn} \tag{140}$$

$$R_2 = \frac{R}{2} (1 + a_m) \sin\theta_{sn} \tag{141}$$

and

$$R_3 = R_1 - x_i - \frac{w}{2} a_\ell \tag{142}$$

Then

$$r = [R_3^2 + (R_2 - a_j\, y_i)^2 + z^2]^{1/2} \tag{143}$$

and

$$\theta_{sn} = \frac{\pi}{8} [2s - 1) + a_n] \tag{144}$$

A.4 Response of the Receiving Transducer in the Presence of Delaminations

The response of the receiving transducer is also governed by Eqn. (128). The formula for H_1 and H_2 in rectangular coordinates are

$$H_1 = \frac{zk}{2\pi} \int_{-R_1}^{R_1} \int_{(R^2-\eta^2)^{1/2}}^{(R^2-\eta^2)^{1/2}} \int_{-R_1}^{R_1} \int_{-(R^2-x^2)^{1/2}}^{(R^2-x^2)^{1/2}} \left(\frac{\sin kr}{r^2} + \frac{\cos kr}{kr^3}\right) d\eta d\gamma dx dy \tag{145}$$

and

$$H_2 = \frac{zk}{2\pi} \int_{-R_1}^{R_1} \int_{-(R^2-\eta^2)^{1/2}}^{(R^2-\eta^2)^{1/2}} \int_{-R_1}^{R_1} \int_{-(R^2-x^2)^{1/2}}^{(R^2-x^2)^{1/2}} \left(\frac{\cos kr}{r^2} - \frac{\sin kr}{kr^3}\right) d\eta d\gamma dx dy \tag{146}$$

where R_1 is the perpendicular distance from the center of the transducer to the inside edge of the delamination, and

$$r = [(x - \eta)^2 + (y - \gamma)^2 + z^2]^{1/2} \tag{147}$$

The approximations for H_1 and H_2 are

$$H_1 = \frac{zR_1^2k}{2\pi} \sum_{i=1}^{16} \sum_{j=1}^{16} \sum_{\ell=1}^{16} \sum_{m=1}^{16} h_i\, h_j\, h_\ell\, h_m\, D_i\, D_j \left(\frac{\sin kr}{r^2} + \frac{\cos kr}{kr^3}\right) \tag{148}$$

and

$$H_2 = \frac{zR_1^2k}{2\pi} \sum_{i=1}^{16} \sum_{j=1}^{16} \sum_{\ell=1}^{16} \sum_{m=1}^{16} h_i\, h_j\, h_\ell\, h_m\, D_i\, D_j \left(\frac{\cos kr}{r^2} - \frac{\sin kr}{kr^3}\right) \tag{149}$$

where

$$D_i = (R^2 - R_1^2\, a_i^2)^{1/2} \tag{150}$$

and

$$r = [R_1^2\,(a_j - a_i)^2 + (D_j\, a_\ell - D_i\, a_k)^2 + z^2]^{1/2} \tag{151}$$

A.5 List of Symbols used in the Programs

The following list defines the relationship between the symbols in the computer programs and the nomenclature in Eqns. (119) through (151)

A (I) : a_i (16-point Gaussian quadrature)

H (I) : h_i (16-point Gaussian quadrature)

Z (I) : z

BETA : k

R : R

H1 : H_1

H2 : H_2

X (I) : x_i

Y (I) : y_i

ABAR (I) : a_i (4-point Gaussian quadrature)

HBAR (I) : h_i (4-point Gaussian quadrature)

H11 : H_1'

H22 : H_2'

P : $\tilde{p}$

RHO : r

A.6 Computer Programs

The following is a listing of the computer programs used in computing the appropriate values of attenuation.

```
C
C
C     THIS PROGRAM CALCULATES THE PRESSURE ALONG THE AXIS OF THE
C     TRANSDUCER IN X-Y COORDINATES.
C     INPUT DATA:
C     H(U) - H(16)  (GAUSSIAN QUADRATURE)          F18.15
C     A(U) - A(16)  (GAUSSIAN QUADRATURE)          F18.15
C     BETA (WAVE NUMBER/PI)                        F18.15
C     R (RADIUS OF THE TRANSDUCER)                 F18.15
C     NZ (SIZE OF THE ARRAY Z)                     I2
C     Z(1) - Z(NZ)                                 F18.15
C
 C     NOTE: ALL DIMENSIONS ARE IN CM.
C
C
      IMPLICIT REAL*8 (A-H,O-Z)
      DIMENSION A(16),H(16),Z(50)
      PI=4.D0*DATAN(1.D0)
      READ(5,500) H,A,BETA,R
      READ(5,510) NZ
      READ(5,500)(Z(I),I=1,NZ)
      BETA=BETA*PI
  500 FORMAT(F18.15)
  510 FORMAT(I2)
      WRITE(6,600) BETA
  600 FORMAT('1',5X,'BETA = ',F12.6//////)
      DO 20 I=1,NZ
      H1=0.D0
      H2=0.D0
      DO 10 J=1,16
      B=DSQRT(1.D0-A(J)**2)*H(J)
      R1=R*R*A(J)**2
```

```
      DO 10 K=1,16
      RHO=DSQRT(R1*(1.D0-A(K)**2)+R*R*A(K)**2+Z(I)**2)
      R2=RHO*RHO
      R3=RHO*R2
      C=DCOS(BETA*RHO)
      S=DSIN(BETA*RHO)
      H1=H1+B*H(K)*(C/BETA/R3+S/R2)
   10 H2=H2+B*H(K)*(C/R2-S/BETA/R3)
      H1=H1*Z(I)*R*R/2.D0/PI*BETA
      H2=H2*Z(I)*R*R/2.D0/PI*BETA
      P=DSQRT(H1**2+H2**2)
      D=DSQRT(R*R+Z(I)**2)
      P1=DSQRT(1.D0+Z(I)**2/D/D-2.D0*Z(I)/D*DCOS(BETA*(D-Z(I))))
  610 FORMAT(5X,5(F10.6,7X))
   20 WRITE(6,610) Z(I),H1,H2,P,P1
      STOP
      END
```

```
C
C
C     THIS PROGRAM CALCULATES THE PRESSURE ALONG THE AXIS OF THE
C     TRANSDUCER IN RADIAL COORDINATES. INPUT DATA IS THE SAME
C     AS IN THE PREVIOUS PROGRAM.
C
C
      IMPLICIT REAL*8 (A-H,O-Z)
      DIMENSION A(16),H(16),Z(50)
      PI=4.DO*DATAN(1.DO)
      READ(5,500) H,A,BETA,R
      READ(5,510) NZ
      BETA=BETA*PI
      READ(5,500)(Z(I),I=1,NZ)
  500 FORMAT(F18.15)
  510 FORMAT(I2)
      DO 5 I=1,16
    5 A(I)=A(I)+1.DO
      WRITE(6,600)
  600 FORMAT('1')
      WRITE(6,620) BETA
  620 FORMAT(5X,'BETA = ',F12.6/////)
      DO 20 I=1,NZ
      H1=0.DO
      H2=0.DO
      DO 10 J=1,16
      RHO=DSQRT(Z(I)**2+A(J)**2*R*R/4.DO)
      R2=RHO*RHO
      R3=R2*RHO
      C=DCOS(BETA*RHO)
      S=DSIN(BETA*RHO)
      H1=H1+A(J)*(S/R2+C/BETA/R3)*H(J)
```

```
 10 H2=H2+A(J)*(C/R2-S/BETA/R3)*H(J)
    H1=H1*BETA*R/2.D0*Z(I)*R/2.D0
    H2=H2*BETA*R/2.D0*Z(I)*R/2.D0
    P=DSQRT(H1**2+H2**2)
    D=DSQRT(R*R+Z(I)**2)
    P1=DSQRT(1.D0+Z(I)**2/D/D-2.D0*Z(I)*DCOS(BETA*(D-Z(I)))/D)
610 FORMAT(5X,5(F10.6,7X))
 20 WRITE(6,610) Z(I),H1,H2,P,P1
    STOP
    END
```

```
C
C
C     THIS PROGRAM CALCULATES THE APPARENT ATTENUATION AT
C     VARIOUS DISTANCES, WITH CRACKS PRESENT.
C     SUBROUTINE SUB1 MUST BE USED IN CONJUNCTION WITH THIS
C     PROGRAM.
C     INPUT DATA:
C     H(1) - H(16) (GAUSSIAN QUADRATURE)          F18.15
C     A(1) - A(16) (GAUSSIAN QUADRATURE)          F18.15
C     R (RADIUS OF THE TRANSDUCER)                F18.15
C     W (ANGULAR FREQUENCY)                       F18.15
C     V (VELOCITY OF SOUND)                       F18.15
C     WID (WIDTH OF THE CRACKS)                   F18.15
C     NC (HALF THE NUMBER OF CRACKS)              I2
C     HBAR(1) - HBAR(4) (GAUSSIAN QUAD.)          F18.15
C     ABAR(1) - ABAR(4) (GAUSSIAN QUAD.)          F18.15
C     NZ (SIZE OF THE ARRAY Z)                    I2
C     Z(1) - Z(NZ)                                F18.15
C
 C     NOTE: ALL DIMENSIONS ARE IN CM.
C
C
      IMPLICIT REAL*8 (A-H,O-Z)
      COMMON R,H1,H2,BETA,H(16),A(16),P,S(2,16),C(2,16),PI
      COMMON S2(2,16),C2(2,16)
      DIMENSION X(50),Y(50),Z(100),P1(100),P2(100),HBAR(4),ABAR(4)
      READ(5,500) H,A,R,W,V,WID
  500 FORMAT(F18.15)
      READ(5,510) NC
  510 FORMAT(I2)
      READ(5,500) HBAR,ABAR
      PI=4.D0*DATAN(1.D0)
```

```
      BETA=W/V
      DELX=R/(NC+.5)
      X(1)=DELX/2.D0
      X(1+NC)=-X(1)
      Y(1)=DSQRT(R*R-X(1)**2)
      Y(1+NC)=Y(1)
      DO 5 I=2,NC
      X(I)=X(I-1)+DELX
      Y(I)=DSQRT(R*R-X(I)**2)
      X(I+NC)=-X(I)
    5 Y(I+NC)=Y(I)
      NC2=2*NC
      WRITE(6,61)
   61 FORMAT('1',T14,'Z',T24,'S',T43,'H1',T73,'H2'/)
      READ(5,510) NZ
      READ(5,500)(Z(I),I=1,NZ)
      DO 6 K=1,2
      T2=PI/4.D0
      T1=PI/4.D0*(2*K-1)
      T3=T1/2.D0
      T4=T2/2.D0
      DO 6 N=1,16
      TN1=T1+A(N)*T2
      TN=T3+A(N)*T4
      S2(K,N)=DSIN(TN1)
      C2(K,N)=DCOS(TN1)
      S(K,N)=DSIN(TN)
    6 C(K,N)=DCOS(TN)
      DO 30 L=1,NZ
      CALL SUB1(Z(L))
      P1(L)=P
      H11=0.D0
```

```
      H22=0.D0
      DO 20 K=1,2
      DO 20 N=1,16
      DO 20 M=1,16
      R1=R/2.D0*(1.D0+A(M))*C(K,N)
      R2=R/2.D0*(1.D0+A(M))*S(K,N)
      B=H(M)*H(N)*(1.D0+A(M))
      DO 25 I1=1,4
      R3=R1-X(I)-WID/2.D0*ABAR(I1)
      B1=B*Y(I)*HBAR(I1)
      DO 25 I=1,NC2
      DO 25 J=1,16
      RHO=DSQRT(R3**2+Z(L)**2+(R2-Y(I)*A(J))**2)
      C1=DCOS(BETA*RHO)/RHO
      S1=DSIN(BETA*RHO)/RHO
      H11=H11+H(J)*B1*C1
   25 H22=H22+H(J)*B1*S1
   20 CONTINUE
      H1=H1-PI*R*R*WID/8.D0*H11
      H2=H2-PI*R*R*WID/8.D0*H22
      WRITE(6,62)H1,H2
   62 FORMAT(T30,D23.16,T60,D23.16/)
   30 P2(L)=DSQRT(H1**2+H2**2)
      WRITE(6,63)
   63 FORMAT('1',T14,'Z',T25,'ALPHA 1',T45,'ALPHA 2',T70,'P1',T90,'P2'/)
      A1=PI*R*R
      PB=A1/BETA*2.D0*PI
      PA=A1*2.D0*PI/BETA
      DO 40 I=1,NZ
      AL1=20.D0*DLOG10(PB/P1(I))
      AL2=20.D0*DLOG10(PA/P2(I))
   64 FORMAT(T10,F8.5,T25,F12.8,T45,F12.8,T65,F12.8,T85,F12.8)
```

```
40 WRITE(6,64) Z(I),AL1,AL2,P1(I),P2(I)
   WRITE(6,70) NC2,WID
70 FORMAT(///T15,'THERE ARE ',I3,' CRACKS,',F8.6,' CM. WIDE.')
   STOP
   END
   SUBROUTINE SUB1(Z)
   IMPLICIT REAL*8(A-H,O-Z)
   COMMON R,H1,H2,BETA,H(16),A(16),P,S(2,16),C(2,16),PI
   COMMON S2(2,16),C2(2,16)
   DO 5 I=1,16
 5 A(I)=A(I)+1.D0
10 H1=0.D0
   H2=0.D0
   Z2=Z**2
   S1=Z*2.D0*PI/BETA/R**2
   DO 20 K=1,2
   DO 20 M=1,16
   DO 20 N=1,16
   RHO1=A(M)*C2(K,N)
   RHO2=(A(M)*S2(K,N)*R/2.D0)**2+Z2
   B=A(M)*H(M)*H(N)
   DO 20 I=1,16
   RHO=DSQRT(R**2/4.D0*(RHO1-A(I))**2+RHO2)
   H1=H1+A(I)*H(I)*B*DCOS(BETA*RHO)/RHO
20 H2=H2+A(I)*H(I)*B*DSIN(BETA*RHO)/RHO
   H1=H1*R**4*PI*PI/16.D0
   H2=H2*R**4*PI*PI/16.D0
   P=DSQRT(H1**2+H2**2)
   WRITE(6,61) Z,S1,H1,H2
61 FORMAT(T10,F8.5,T20,F8.5,T30,D23.16,T60,D23.16)
   DO 30 I=1,16
30 A(I)=A(I)-1.D0
```

```
      RETURN
      END
```

```
C
C
C     THIS PROGRAM CALCULATES THE ATTENUATION IN THE PRESENCE
C     OF DELAMINATIONS.
C     INPUT DATA:
C     H(1) - H(16) (GAUSSIAN QUAD.)                    F18.15
C     A(1) - A(16) (GAUSSIAN QUAD.)                    F18.15
C     BETA (WAVE NUMBER/PI)                            F18.15
C     R (RADIUS OF THE TRANSDUCER)                     F18.15
C     R1 (DISTANCE FROM CENTER OF TRANSDUCER
C         TO THE EDGE OF THE DELAMINATION)              F18.15
C     NZ (THE SIZE OF THE ARRAY Z)                      I2
C     Z(1) - Z(NZ)                                      F18.15
C
 C     NOTE: ALL DIMENSIONS ARE IN CM.
C
C
      IMPLICIT REAL*8 (A-H,O-Z)
      DIMENSION A(16),H(16),D(16),Z(25)
      PI=4.D0*DATAN(1.D0)
      READ(5,500)H,A,BETA,R,R1
      READ(5,510)NZ
      READ(5,500)(Z(I),I=1,NZ)
  500 FORMAT(F18.15)
  510 FORMAT(I2)
      BETA=BETA*PI
      DO 5 I=1,16
    5 D(I)=DSQRT(R*R-R1*R1*A(I)**2)
      WRITE(6,600) BETA,R1,R
  600 FORMAT('1',5X,'BETA = ',F12.6//5X,'R1 = ',F12.6,5X,'R = ',F12.6//)
      DO 20 M=1,NZ
      H1=0.D0
```

```
      H2=0.D0
      Z1=Z(M)
      DO 10 I=1,16
      B=H(I)*D(I)
      DO 10 K=1,16
      E=B*H(K)*D(K)
      RR=R1*R1*(A(K)-A(I))**2+Z1*Z1
      DO 10 J=1,16
      F=E*H(J)
      DO 10 L=1,16
      RHO=DSQRT(RR+(D(K)*A(L)-D(I)*A(J))**2)
      R2=RHO*RHO
      R3=R2*RHO
      C=DCOS(BETA*RHO)
      S=DSIN(BETA*RHO)
      H1=H1+F*H(L)*(S/R2+C/BETA/R3)
   10 H2=H2+F*H(L)*(C/R2-S/BETA/R3)
      H1=H1*R1*R1*Z1*BETA/2.D0/PI
      H2=H2*R1*R1*Z1*BETA/2.D0/PI
      P=DSQRT(H1**2+H2**2)
      ALPHA=20.D0*DLOG10(PI*R*R/P)
  610 FORMAT(5X,5(F12.6,7X))
   20 WRITE(6,610) Z1,H1,H2,P,ALPHA
      STOP
      END
```